Received 9 October 2020; revised 23 November 2020; accepted 5 December 2020. Date of publication 9 December 2020; date of current version 5 January 2021.

Digital Object Identifier 10.1109/OJCOMS.2020.3043598

Novel Iterative Clipping and Error Filtering Methods for Efficient PAPR Reduction in 5G and Beyond

SELAHATTIN GÖKCELI [1] (Member, IEEE), TONI LEVANEN [2] (Member, IEEE), TANELI RIIHONEN [1] (Member, IEEE), JUHA YLI-KAAKINEN [1], ALBERTO BRIHUEGA [1] (Graduate Student Member, IEEE), MATIAS TURUNEN [1] (Student Member, IEEE), MARKKU RENFORS [1] (Life Fellow, IEEE), AND MIKKO VALKAMA [1] (Senior Member, IEEE)

[1]Department of Electrical Engineering, Tampere University, 33720 Tampere, Finland

[2]Nokia Mobile Networks, Tampere, FI-33100 Finland

CORRESPONDING AUTHOR: S. Gökceli (e-mail: selahattin.gokceli@tuni.fi)

This work was supported in part by the Academy of Finland under Grant 332361 and Grant 319994, in part by Business Finland under the project 5G-VIIMA, in part by Nokia Corporation, and in part by Tampere University Graduate School.

ABSTRACT The physical-layer radio access of 5G New Radio (NR) and other modern wireless networks builds on the cyclic prefix (CP) orthogonal frequency-division multiplexing (OFDM), known to suffer from the high peak-to-average power ratio (PAPR) challenge. In this article, novel PAPR reduction methods are developed, referred to as the iterative clipping and weighted error filtering (ICWEF) approach. To this end, clipping noise is separated from the data signal in frequency domain and properly tailored frequency-selective clipping noise filtering is adopted to control the tradeoff between PAPR reduction and transmitted signal quality. Furthermore, as 5G NR networks support adopting different OFDM numerologies at different bandwidth parts within one channel bandwidth, the ICWEF approach is also extended to take into account and suppress the resulting inter-numerology interference—something that most existing state-of-the-art methods do not consider. To facilitate comprehensive performance evaluations, a software-defined radio based prototyping testbed including a high-power base station power amplifier is also developed and used for assessing the performance of PAPR reduction solutions. The proposed ICWEF-based PAPR reduction concept is thereon thoroughly validated with extensive numerical and experimental results and shown to outperform the existing state-of-the-art reference solutions.

INDEX TERMS 5G new radio (NR), clipping, error vector magnitude (EVM), filtering, mixed numerology, orthogonal frequency-division multiplexing (OFDM), peak-to-average-power ratio (PAPR), prototyping, software-defined radio (SDR), waveform, wireless communications.

I. INTRODUCTION

FIFTH generation (5G) mobile networks, most notably 3GPP 5G New Radio (NR), are expected to provide substantial connectivity improvements in terms of data rate, reliability, latency, and energy consumption [1], [2]. The physical-layer radio access of the 5G NR is based on cyclic prefix (CP) orthogonal frequency-division multiplexing (OFDM) due to its various benefits such as efficient multiple-input multiple-output (MIMO) support and flexibility in the frequency-domain resource allocation granularity. However, the high peak-to-average power ratio (PAPR) is one important drawback of the CP-OFDM waveform and may easily hinder from achieving the targeted improvements with 5G if not properly handled. In line with this, the PAPR problem has been investigated extensively in the literature and some well-known PAPR reduction methods are iterative clipping and filtering (ICF) [3], selected mapping [4], tone reservation (TR) [5], and partial transmit sequence [6]. Detailed descriptions of these methods and some other alternatives are available in [7].

As one of the most effective methods among the well-known PAPR reduction methods, ICF provides a straightforward PAPR reduction mechanism by iterative implementation of clipping in time domain and clipping noise filtering in frequency domain to null the out-of-band (OOB) emissions caused by the clipping noise [8]. This filtering operation is based on the weighting of the subcarriers (SCs) of the clipped signal in frequency domain and, in the conventional ICF solutions, clipping noise is spread evenly over all active subcarriers.

However, traditional ICF filtering model is problematic for 3GPP Long Term Evolution (LTE)/LTE-Advanced and 5G NR networks as aggressive frequency-domain multiplexing of users with highly different quality-of-service expectations is utilized [1], [2]. Furthermore, physical resource block (PRB) level control of the modulation and coding scheme (MCS) is a common feature of modern networks. Therefore, frequency-selective distribution of the clipping noise over the active PRBs should be supported. In accordance with this requirement, iterative clipping and error filtering (ICEF) method was introduced in [9]. This method is based on the separation of clipping noise from data signal in frequency domain and the clipping noise inside the active subcarriers is controlled at PBR level by using a proposed frequency-domain mask. However, the study in [9] does not set any constraint on the clipping noise level. This, in turn, can cause problems as particular PRBs would require high MCS and in this case, clipping noise level should be limited for these PRBs. Similarly, some PRBs might tolerate a high clipping noise level and, if clipping noise is uniformly distributed over the active PRBs, desired PAPR reduction performance may not be obtained. The methods developed in this article facilitate such controlled MCS-specific clipping noise weighting at different passband PRBs, going thus beyond the state-of-the-art.

In general, the 5G NR use cases may necessitate different OFDM numerologies being adopted inside one NR carrier—commonly called the mixed-numerology support [1], [2]. This causes an additional challenge as inter-numerology interference (INI) emerges [10]. Properly handling the INI is, in general, critical while the PAPR problem of CP-OFDM becomes also more challenging in mixed-numerology scenarios. Specifically, the subband CP-OFDM signals already suffer from high PAPR and, even if separate PAPR reduction is applied on each subband signal, final combination of the subband signals renders a significant increase in the total waveform PAPR. The PAPR reduction problem in mixed-numerology systems was introduced and preliminary addressed in [11], while a more comprehensive and efficient formulation of the mixed-numerology PAPR suppression is presented in this article.

A. RELATED WORKS

The recent studies on ICF have mainly focused on the minimization of both PAPR and distortion caused by clipping noise. For example, in [12], to reduce the complexity of convex optimization based approaches, a method that creates a time-domain kernel matrix to provide a good tradeoff between PAPR reduction and error vector magnitude (EVM) performance is proposed. Moreover, peak cancellation is applied in time domain, thus preventing an increase of the complexity. In [13], same performance metrics are considered and an efficient optimization procedure is targeted by using linearized alternating direction method of a multipliers algorithm.

In [14], complexity reduction of the clipping-based PAPR reduction methods is targeted and an efficient time-domain PAPR reduction mechanism based on the designed compression algorithm is proposed. In [15], a comprehensive methodology is proposed to reduce the PAPR efficiently and limit the degradation in the bit error rate (BER) performance. The procedure is based on changing the amplitude distribution to uniform distribution and an additional optimization routine is also applied to limit the number of iterations. Moreover, in [16], by considering carrier aggregation scenarios, a convex optimization-based filter design is proposed for ICF method to obtain a good tradeoff between PAPR and BER performance.

In [17], a frequency-selective clipping noise filtering design is proposed for different PAPR reduction methods that are applied on carrier-aggregated signals. The presented results show the effectiveness of the MSE-based limitation of clipping noise and possible gains that can be obtained with this approach. In [17], a prototype filter design is considered; however, such an approach may not be feasible due to the complexity issues and limited flexibility in terms of the options for the clipping noise filter. Therefore, a more comprehensive design is required for the effective utilization of frequency-selective modulation-specific clipping noise filtering.

Only few studies in the open literature have so far coped with the PAPR reduction problem in mixed-numerology (MN) systems. In [18], PAPR is analyzed for MN-based transmission and an analytical expression based on level-crossing theory is derived for the probability distribution of PAPR. In [19], PAPR reduction problem of mixed-numerology transmission is targeted and an ICF-based method, which comprises INI cancellation, is proposed for the mixed-numerology case. Moreover, different optimization routines are proposed to improve the PAPR performance further for this case. One important issue is that frequency-selective clipping noise filtering is not considered in the study. Since PRB-level allocation of MCS is a prominent concept in 5G NR, frequency-selective allocation of clipping noise is required and, considering the high number of possibilities related to the PRB-level MCS allocation in mixed-numerology transmission, running optimization routines for every possible allocation would be very complicated and thus highly undesirable. To the best of the authors' knowledge, there is not any comprehensive study in the literature proposing extensive solutions for effective realization of frequency-selective clipping noise filtering in both single-numerology and mixed-numerology systems, such that the transmit signal quality in terms of clipping noise can be efficiently controlled at PRB level.

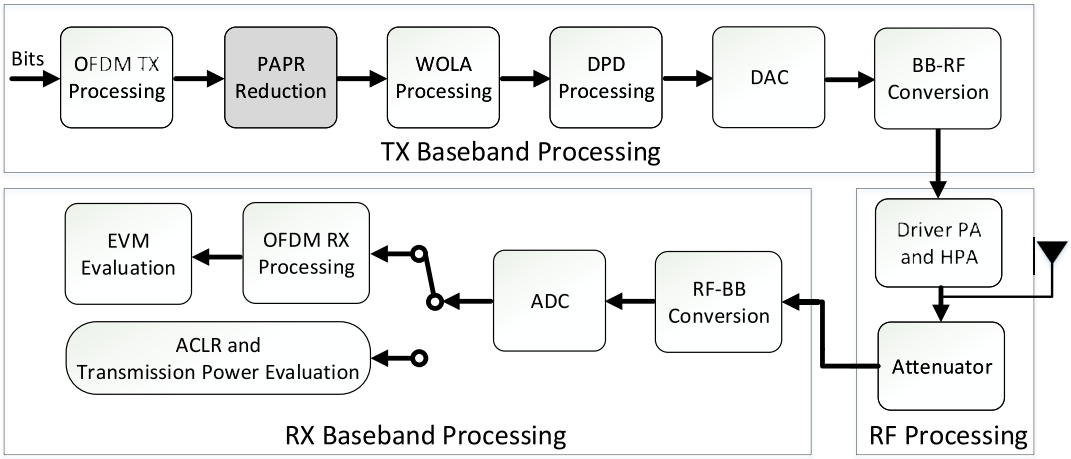

FIGURE 1. Overall considered system model at high-level where the main TX processing blocks are shown. The PAPR reduction block is high-lighted in grey. The figure also shows relevant RX processing blocks in order to evaluate the transmit signal quality by using a test receiver.

B. CONTRIBUTIONS OF THIS ARTICLE

In this article, frequency-selective PAPR reduction in both single-numerology and mixed-numerology CP-OFDM systems is studied and developed to a new sophisticated level. The contributions of this article can be summarized as follows:

- The so-called iterative clipping and weighted error filtering (ICWEF) method is proposed to effectively reduce the PAPR in single-numerology CP-OFDM systems, while facilitating precise PRB-level clipping noise control.
- Moreover, mixed-numerology ICWEF (MN-ICWEF) and MN-ICWEF with inter-numerology-interference cancellation (MN-ICWEF-INIC) are also proposed for PAPR reduction in mixed-numerology based CP-OFDM systems.
- In line with the corresponding 5G NR requirements, the proposed PAPR reduction mechanisms are shown to satisfy the in-band MCS-specific MSE requirements while also allow for efficiently controlling the clipping noise in the out-of-band (OOB) emission region.
- Comprehensive numerical and experimental performance evaluations are presented by following the associated 5G NR requirements and related performance metrics. Results are discussed and analyzed with respect to the 3GPP specifications and the compatibility of the proposed methods to 5G NR requirements is investigated and demonstrated.
- An actual software-defined radio (SDR) prototype is also implemented to evaluate the performance of the PAPR reduction methods through RF measurements. In the SDR prototype, a true macro base-station high-power amplifier (HPA) is adopted, together with a digital predistortion (DPD) unit [20], [21], in order to reach true downlink (DL) transmit power levels in the order of +50 dBm in the study, and to be able to realistically measure the impact of the PAPR reduction algorithms on the different 5G NR DL emission measurements.

Overall, this article provides substantial contributions in the field of novel PAPR reduction techniques in 5G NR networks, facilitating increased system power efficiency and increased transmit power levels while offering flexible and computationally efficient solutions to control the transmitted waveform quality in both single-numerology and mixed-numerology networks.

C. ORGANIZATION OF THIS ARTICLE

The rest of this article is organized as follows. In Section II, basic system models of the CP-OFDM transceiver processing and ICF reference method are given. In Section III, the proposed ICWEF technique is introduced and described, complemented with some numerical performance results for selected single-numerology scenarios. In Section IV, the mixed-numerology extension is addressed, and the corresponding MN-ICWEF and MN-ICWEF-INIC methods are described. In Section V, detailed analysis of the computational complexities of the different methods is provided. Then, in Section VI, the developed SDR testbed and the relevant 5G NR transmit signal quality metrics are described. Then, in Section VII, both simulation-based as well as measurement-based results are presented and analyzed, together with quantitative processing complexity numbers. Finally, the study is concluded in Section VIII.

II. SYSTEM MODEL

A high-level block-diagram or system model is shown in Fig. 1, where the main modules in the considered transmitter (TX) system are shown. Basically, the TX-side OFDM processing and PAPR reduction are consecutively realized with different structures based on the use scenario, which will be detailed in the following sections. Afterwards, weighted

overlap-and-add (WOLA) processing for improving the spectrum localization and DPD processing for controlling (H)PA nonlinearities are applied. Then, digital-to-analog conversion (DAC) and baseband-to-RF conversion are applied, followed by a driver PA and an actual HPA. In receiver (RX) processing, shown here mostly for transmit signal quality measurement purposes, RF-to-baseband conversion and analog-to-digital conversion (ADC) are applied, and RX-side OFDM processing is realized. Then, performance metrics such as EVM, ACLR, and transmission power level are evaluated.

A. CP-OFDM SIGNAL MODEL

Considering for generality the allocation of multiple BWPs, the number of subbands is M and the OFDM transform size on subband m for $m \in \{0, 1, \ldots, M-1\}$ is denoted by $N_{\text{OFDM},m}$. The number of active subcarriers $N_{\text{act},m}$ on subband m is bounded by the OFDM transform size, i.e., $N_{\text{act},m} < N_{\text{OFDM},m}$. It is assumed that the active subcarriers are located symmetrically around the DC bin when double-sided bins and subcarrier indexing is considered. In the model, oversampling, which is a key for accurate approximation of the true analog waveform [22], is applied and oversampled inverse discrete Fourier transform (IDFT) size is denoted by $N_m = N_{\text{OFDM},m} N_{\text{ov}}$ with oversampling factor of N_{ov}. Let us denote by $X_{m,s}[k]$ the data symbol at the active subcarrier $k \in \{-N_{\text{act},m}/2, \ldots, N_{\text{act},m}/2 - 1\}$ of the sth OFDM symbol for $s \in \{0, 1, \ldots, S_m - 1\}$ on subband m.

In "OFDM TX processing" shown in Fig. 1, the initial discrete-time OFDM symbol samples are obtained through IDFT as denoted by

$$x_{m,s}[n] = \frac{1}{\sqrt{N_{\text{act},m}}} \sum_{k=-N_{\text{act},m}/2}^{N_{\text{act},m}/2-1} X_{m,s}[k] e^{j2\pi kn/N_m}, \tag{1}$$

where n corresponds to the relative time-domain sample index inside the OFDM symbol, i.e., $n = 0, 1, \ldots, N_m - 1$. The OFDM TX processing is finalized with the CP addition and the parallel-to-serial conversion. This processing for the mth subband can be compactly expressed as

$$\mathbf{x}_m = \text{vec}\left(\mathbf{T}_{\text{CP},m} \mathbf{W}_{N_m}^{-1} \mathbf{X}_m\right), \tag{2}$$

where $\mathbf{X}_m$ is the $N_m \times S_m$ matrix that contains frequency-domain symbols and $\mathbf{W}_{N_m}^{-1}$ is the $N_m \times N_m$ IDFT matrix. Moreover, $\mathbf{T}_{\text{CP},m}$ represents the $(N_m + N_{\text{CP},m}) \times N_m$ CP insertion matrix with $N_{\text{CP},m}$ being the oversampled CP length, and $\text{vec}(\cdot)$ represents vectorization operation. In the continuation, "PAPR reduction" in Fig. 1 is realized based on the corresponding use case. Finally, "WOLA Processing" in Fig. 1 is applied and the output signal is obtained as

$$\mathbf{x} = \sum_{m=0}^{M-1} \mathbf{K}_m \mathbf{x}_m, \tag{3}$$

where $\mathbf{K}_m$ is TX-side WOLA processing and it consists of submatrices realizing symbol length extension and windowing, as described in [23]. Next, "DPD processing" in Fig. 1 is also applied to satisfy the 5G NR DL ACLR limit with a realistic HPA. With "DAC" and "BB-RF Conversion" blocks, "TX Basedband Processing" in Fig. 1 is concluded.

Afterwards, as shown in "RF Processing" in Fig. 1, the power of the signal is amplified to a significantly high level by using a driver PA and a HPA. When observing the transmit waveform, an attenuator is applied to decrease the power level to an acceptable level based on the RX device's input power limit.

In the "RX Basedband Processing" in Fig. 1, first, "RF-BB Conversion" and "ADC" blocks are realized. Afterwards, in "OFDM RX Processing", serial-to-parallel conversion and CP removal are applied and received frequency-domain samples for mth subband and sth symbol are obtained after DFT as

$$Y_{m,s}[k] = \sqrt{N_{\text{act},m}} \sum_{n=0}^{N_m-1} y_{m,s}[n] e^{-j2\pi kn/N_m}, \tag{4}$$

where $y_{m,s}[n]$ represents the nth time-domain sample of the received signal from the channel without CP. In the following steps, channel estimation and equalization are realized and, "OFDM RX Processing" is finalized. To evaluate the performance, EVM as well as MSE are calculated. Moreover, ACLR and transmission power are measured with the test RX when that option is selected, which correspond to last steps of "RX Baseband Processing."

B. TRADITIONAL ICF METHOD FOR PAPR REDUCTION

The initial CP-OFDM waveform obtained using (1) is used as an input at the first iteration of the ICF-based processing [3]. By introducing the iteration index $l \in \{1, 2, \ldots, \mathcal{L}\}$, nth sample of mth subband and sth time-domain CP-OFDM symbol can be denoted as $x_{m,s}^{(l)}[n]$ while $x_{m,s}^{(0)}[n]$ denotes the initial waveform. Here $\mathcal{L}$ is the maximum number of iterations. Then, the sample-wise PAPR of $\mathbf{x}_m^{(l)}$ over the $S_m N_m$ samples is defined as

$$\text{PAPR}\left(\mathbf{x}_m^{(l)}\right) = 10 \log_{10} \frac{\max_{n=0,1,\ldots,S_m N_m - 1} \left\{ |x_m^{(l)}[n]|^2 \right\}}{\frac{1}{S_m N_m} \sum_{n=0}^{S_m N_m - 1} |x_m^{(l)}[n]|^2}, \tag{5}$$

where $\max\{\cdot\}$ is the maximum operator and $x_m^{(l)}[n]$ is the nth sample of $\mathbf{x}_m^{(l)}$.

The PAPR target is denoted by λ_{target} ($\lambda_{\text{target,dB}}$ denotes it in dB scale) . The soft limiter based clipping operation is defined as

$$\bar{x}_{m,s}^{(l)}[n] = \begin{cases} A^{(l-1)} e^{j \angle x_{m,s}^{(l-1)}[n]}, & \text{if } \left| x_{m,s}^{(l-1)}[n] \right| > A^{(l-1)} \\ x_{m,s}^{(l-1)}[n], & \text{otherwise} \end{cases} \tag{6}$$

where $\angle x$ and $|x|$ denote the phase angle and modulus of a complex number x, respectively. Moreover, $\bar{x}_{m,s}^{(l)}[n]$ is the clipped $x_{m,s}^{(l-1)}[n]$ and $A^{(l-1)}$ is the amplitude threshold value that is computed as

$$A^{(l-1)} = \sqrt{\lambda_{\text{target}} \, \text{E}\left(\left| \mathbf{x}_m^{(l-1)} \right|^2 \right)}, \tag{7}$$

where E(·) is the expectation operator. Here, clipping function in (6) is considered as the step that starts the next iteration, which is shown by increasing the iteration index by one in this step.

After (6), frequency-domain samples are obtained by computation of DFT of size N_m providing the frequency-domain presentation of the clipped signal defined as $\mathbf{X}_{m,s}^{(l)} = \mathbf{W}_{N_m}\bar{\mathbf{x}}_{m,s}^{(l)}$. Then, frequency-domain filtering is applied to suppress the clipping noise outside the passband region. The implemented ICF frequency-domain filter mask in the filtering phase can be defined as

$$H_{\mathrm{ICF}}[k] = \begin{cases} 1, & \text{if } k \in \mathcal{K}_{\mathrm{act},m}, \\ 0, & \text{if } k \in \mathcal{K}_{\mathrm{null},m}, \end{cases} \tag{8}$$

where $\mathcal{K}_{\mathrm{act},m}$ and $\mathcal{K}_{\mathrm{null},m}$ are the sets that contain the active SCs and non-active SCs, respectively, and the cardinality of the union of the sets is equal to N_m, i.e., $\mathrm{card}(\mathcal{K}_{\mathrm{act},m} \cup \mathcal{K}_{\mathrm{null},m}) = N_m$, where $\mathrm{card}(\cdot)$ is the cardinality of the set. The frequency-domain filtering operation at iteration l is represented as

$$X_{m,s}^{(l)}[k] = H_{\mathrm{ICF}}[k]\bar{X}_{m,s}^{(l)}[k], \tag{9}$$

and finally the time-domain signal is obtained as $\mathbf{x}_{m,s}^{(l)} = \mathbf{W}_{N_m}^{-1}\mathbf{X}_{m,s}^{(l)}$. As it can be seen from (8) and (9), the applied frequency-domain filtering only processes clipping noise outside passband, and the passband clipping noise is not processed, resulting in uniform passband distortion. Furthermore, clipping noise processing is applied on the clipped signal and this limits the filter masks that can be utilized, as changing the amplitude value of the clipped signal would cause increase in BER. Therefore, only limited passband noise suppression gains can be obtained with the traditional ICF approach.

III. PROPOSED ITERATIVE CLIPPING AND WEIGHTED ERROR FILTERING (ICWEF) METHOD

A. BACKGROUND

The ICEF method presented in [9] targets to overcome the limitations caused by filtering the clipped signal in traditional ICF. The frequency-selective clipping noise filtering is achieved by separating the clipping noise from the data signal and adopting the corresponding frequency-domain filtering. Frequency-domain mask can be freely and flexibly chosen based on the considered allocation. With ICEF in [9], clipping noise is allowed only in specific PRBs in accordance with the MSE requirements defined for these PRBs and remaining ones are allocated as clipping noise-free PRBs.

When PRB-level control of MCS is required, traditional ICF cannot be directly applied, because each modulation has different quality-of-service requirement and each PRB is supported with a specific modulation order. Since modulations have certain MSE requirements, error performance is limited with the corresponding MSE level. In this article, we follow the EVM limits defined in [24], which correspond to 17.5%, 12.5%, 8%, and 3.5% for QPSK, 16-QAM, 64-QAM, and 256-QAM, respectively. The corresponding MSE values in decibels are defined as $\mathrm{MSE} = 20\log_{10}(\mathrm{EVM}/100)$. Therefore, an appropriate noise mask that limits noise power level to the corresponding threshold is a necessity. This is especially important on the base station side processing, where in each subframe a new scheduling decision is made, defining which PRBs are allocated to which users with specific MCS. Therefore, the considered frequency-domain mask should not be considered as a static one, but as something that changes with the scheduling resolution of the system.

The ICEF method introduced in [9] contains some limitations and thus a more generalized and efficient PAPR reduction solution for the highlighted issues is pursued. Firstly, only trivial binary weights from frequency domain control of clipping noise were considered in the ICEF in [9]. Furthermore, the utilization of the guardbands in the clipping noise processing was not considered in the original ICEF solution and this is an important feature for different 5G use cases, as the efficient usage of the available bandwidth is desired. In accordance with this, while allowing for the frequency-selective modulation-specific clipping noise filtering, instead of trivial weights, the ICWEF method targets allocation of clipping noise to inband guardbands (viz. those between the BWPs) and also guardbands at the edges of the channel bandwidth. This way, allocated bandwidth is effectively exploited in the PAPR reduction and a good PAPR performance can be achieved.

B. PROPOSED METHOD

In ICWEF, the clipping noise at iteration l can be obtained in frequency domain as

$$C_{m,s}^{(l)}[k] = \bar{X}_{m,s}^{(l)}[k] - X_{m,s}^{(0)}[k]. \tag{10}$$

Then, the extracted clipping noise is filtered with an ICWEF mask. In the filtering phase of the ICWEF method, some or all subcarriers are used to carry clipping noise and the remaining ones are allocated as clipping noise-free subcarriers, which are contained in the subcarrier set $\mathcal{K}_{\mathcal{F},m}$. It is assumed that subcarriers in $\mathcal{K}_{\mathcal{F},m}$ are exploited either to support very high-order modulations, e.g., 1024-QAM, or to improve the reliability by reducing TX EVM, e.g., for ultra-reliable low-latency communication (URLLC) signals.

In the baseline ICEF method in [9], for reference, the active band subcarriers set $\mathcal{K}_{\mathrm{act},m}$ is divided into two sets, which are $\mathcal{K}_{\mathcal{E},m}$ and $\mathcal{K}_{\mathcal{F},m}$. Here, $\mathcal{K}_{\mathcal{E},m}$ is the set that contains passband SCs where clipping noise is allowed. Based on this, frequency-selective filtering is achieved with ICEF as [9]

$$H_{\mathrm{ICEF},m}[k] = \begin{cases} 1, & \text{if } k \in \mathcal{K}_{\mathcal{E},m}, \\ 0, & \text{if } k \in \mathcal{K}_{\mathcal{F},m} \cup \mathcal{K}_{\mathrm{null},m}. \end{cases} \tag{11}$$

Here, it is clear that clipping noise level is not limited for $\mathcal{K}_{\mathcal{E},m}$ and this would cause some inefficiencies as target

clipping level should be high enough to prevent the violation of EVM requirements.

However, in the ICWEF model, set $\mathcal{K}_{\text{act},m}$ is considered as the combination of clipping noise-free subcarriers and active subcarrier set of each modulation, i.e.,

$$\mathcal{K}_{\text{act},m} = \mathcal{K}_{\mathcal{F},m} + \sum_{i=1}^{\text{card}(\mathcal{K}_{\mathcal{M}})} \mathcal{K}_{\mathcal{M}_i,m}, \tag{12}$$

where $\mathcal{K}_{\mathcal{M}_i,m}$ is the index set that contains the subcarriers that are modulated with ith modulation of the modulation set $\mathcal{K}_{\mathcal{M}}$. For example, one can assume that $\mathcal{K}_{\mathcal{M}}$ consists of four different modulations, with $i \in [1, 2, 3, 4]$ corresponding to QPSK, 16-QAM, 64-QAM, and 256-QAM modulations, respectively. In this case, if all four modulations are used for particular PRBs which are allocated for mth subband signal, then there will be four different sets of $\mathcal{K}_{\mathcal{M}_i,m}$. Based on this, in the ICWEF method, following filtering model is applied:

$$H^{(l)}_{\text{ICWEF},i,m}[k] = \begin{cases} \frac{E_i}{\left|C^{(l)}_{m,s}[k]\right|}, & \text{if } k \in \mathcal{K}_{\mathcal{M}_i,m} \wedge E_i < \left|C^{(l)}_{m,s}[k]\right|, \\ 1, & \text{if } k \in \mathcal{K}_{\mathcal{M}_i,m} \wedge E_i \geq |C^{(l)}_{m,s}[k]|, \\ 0, & \text{if } k \notin \mathcal{K}_{\mathcal{M}_i,m}. \end{cases} \tag{13}$$

Here, E_i denotes the weight that limits the clipping noise power to corresponding EVM threshold of ith modulation and can be computed as $E_i = \frac{\text{EVM}_i(\%)}{100}$, where $\text{EVM}_i(\%)$ represents the EVM limit of ith modulation as percentage. In result, ICWEF filter that is applied in lth iteration is obtained as the summation of all $H^{(l)}_{\text{ICWEF},i,m}[k]$ filters as

$$H^{(l)}_{\text{ICWEF},m}[k] = \sum_{i=1}^{\text{card}(\mathcal{K}_{\mathcal{M}})} H^{(l)}_{\text{ICWEF},i,m}[k]. \tag{14}$$

A visual demonstration of a sample frequency-domain mask is shown in Figure 2. In this particular example, from left to right side of the figure, QPSK, 64-QAM, 16-QAM, and 256-QAM modulations are utilized for 43, 10, 16, and 37 PRBs, respectively. Here, 5G NR error quality requirements are followed [24]. In addition to the given EVM requirements for modulations, a 2% EVM margin is also considered. Other TX impairments cause a noticeable increase in EVM and additional error should be taken into account, which is assumed as 2% EVM in the implementation. Thus, MSE limits are obtained as approximately -16.2, -19.6, -24.5 and -36.5 dB for QPSK, 16-QAM, 64-QAM, and 256-QAM, respectively. The magnitude of the frequency-domain mask in Fig. 2 corresponds to the error quality requirements of the used modulations and these thresholds limit the clipping noise power. In this way, desired user-specific MSE performance is obtained.

After the filtering phase, the filtered clipping noise is added back to the original non-clipped signal, expressed in frequency domain as

$$X^{(l)}_{m,s}[k] = X^{(0)}_{m,s}[k] + H^{(l)}_{\text{ICWEF},m}[k] C^{(l)}_{m,s}[k], \tag{15}$$

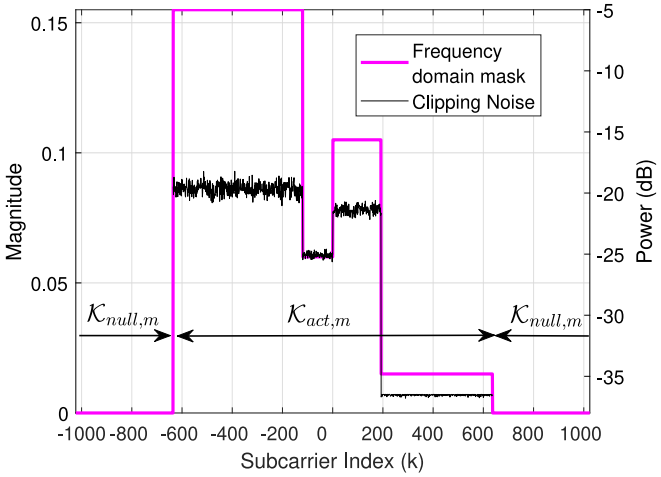

FIGURE 2. An example frequency-domain mask. Here, only active band subcarriers in $\mathcal{K}_{\text{act},m}$ carry clipping noise and clipping noise power levels are different for PRBs utilizing different modulation orders.

and the time-domain signal is obtained after IDFT, i.e., $\mathbf{x}^{(l)}_m = \mathbf{W}^{-1}_{N_m}\mathbf{X}^{(l)}_m$. The subsequent processing stages, such as CP addition, are implemented as in any OFDM TX.

Algorithm 1 summarizes the overall processing flow that is executed for every OFDM symbol while using vector notation for presentation convenience. At the end of the processing, the PAPR-reduced signal $\mathbf{x}^{(\mathcal{L})}_m$ is obtained, which reads

$$\mathbf{x}^{(\mathcal{L})}_m = \text{vec}\left(\mathbf{T}_{\text{CP},m}\mathbf{W}^{-1}_{N_m}\mathbf{X}^{(\mathcal{L})}_m\right). \tag{16}$$

Separate processing of the filtered clipping noise or peak cancellation signal is as an additive element to the original ICF processing and this is the most important feature of the algorithm. The conventional ICF can be seen as a special case of ICWEF with $\mathcal{K}_{\mathcal{F},m} = \emptyset$ and all filter coefficients are equal to one. This means that clipping noise is distributed over all active SCs without considering EVM requirements. Moreover, as shown in (8), the overall passband width (size of $\mathcal{K}_{\text{act},m}$) is the only parameter that changes the applied mask in ICF.

Similarly, the filter shown in (11) can be considered as a special case of ICWEF as well, where utilization of low order modulations and targeting high PAPR level with ICWEF would result in ICEF filter. However, this would be inefficient as PAPR level cannot be reduced much to satisfy the corresponding EVM requirements. Even if some PRBs are modulated with a low-order modulation, due to usage of a simple mask with values of 0 and 1 as weights, clipping noise level needs to be tuned to a lower level than the achievable level. On the other hand, this is not valid for ICWEF. As it can be seen from the given equations, clipping noise allocation is achieved effectively and PAPR reduction gain is maximized. Moreover, in ICWEF, iterations might result in different filter coefficients and filter coefficients are updated in the iteration phase to improve the PAPR reduction performance.

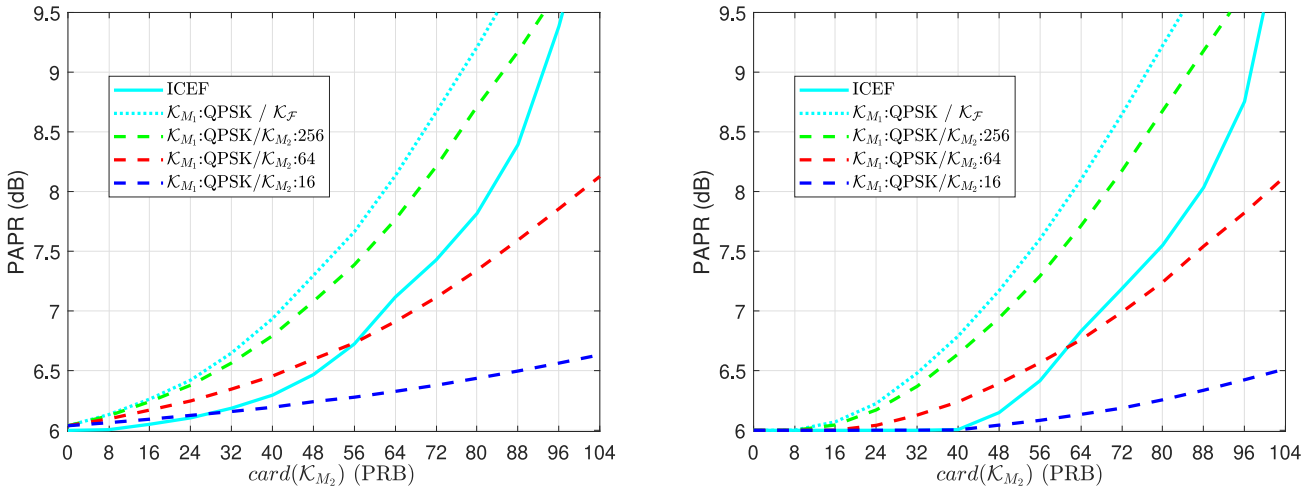

FIGURE 3. PAPR performance results at CCDF level of 1% in different ICWEF cases for different PRB allocation cases, with 10 iterations in (a) and with 20 iterations in (b). The ICEF algorithm [9] is also evaluated as a reference.

Algorithm 1 ICWEF Algorithm for Single-Numerology Operation

1: Set $\mathcal{K}_{\mathcal{M}_i,m}$, $\mathcal{K}_{\mathcal{M}}$, $\mathcal{K}_{\mathcal{F},m}$ and $\mathcal{K}_{\text{null},m}$
2: Set $l = 0$
3: Compute PAPR($\mathbf{x}_m^{(l)}$) according to (5)
4: **if** (PAPR($\mathbf{x}_m^{(l)}$) $> \lambda_{\text{target,dB}}$) **and** ($l < \mathcal{L}$) **then**
5: Set $l = l + 1$
6: Compute $\bar{\mathbf{x}}_m^{(l)}$ according to (6)
7: Compute $\bar{\mathbf{X}}_m^{(l)} = \mathbf{W}_{N_m}^{-1}\bar{\mathbf{x}}_m^{(l)}$
8: Compute $\mathbf{C}_m^{(l)}$ according to (10)
9: Create $\mathbf{H}_{\text{ICWEF},i,m}^{(l)}$ according to (13)
10: Create $\mathbf{H}_{\text{ICWEF},m}^{(l)}$ according to (14)
11: Compute $\mathbf{X}_m^{(l)}$ according to (15)
12: Compute $\mathbf{x}_m^{(l)} = \mathbf{W}_{N_m}\mathbf{X}_m^{(l)}$
13: **Go to step** 3
14: **else**
15: return $\mathbf{x}_m^{(l)}$
16: **end if**

C. PERFORMANCE EXAMPLES WITH DIFFERENT CLIPPING ERROR THRESHOLDS

In this section, numerical performance results are presented and analyzed for the ICWEF scheme. Simulation parameters that are configured by following the 5G NR radio interface numerology defined in [24], are given in Table 1. Accordingly, 20 MHz NR channel bandwidth is considered and the total number of active SCs is configured as $N_{\text{act}} = 1272$, or 106 PRBs with 12 SCs each. Since only one subband is considered for the time being, subband index m is omitted in this discussion. To quantify PAPR performance, complementary cumulative distribution function (CCDF) that represents the probability of signal's envelope being above a threshold [7], is used to quantify the PAPR reduction performance. In this evaluation, PAPR target level of 6 dB and CCDF level of 1% are considered as the reference levels.

TABLE 1. Simulation and evaluation parameters used in ICWEF performance evaluation that is presented in Section III-C.

Parameter	Value
Number of subbands (M)	1
PRB size	12 SCs
Number of active SCs ($N_{\text{act},m}$) / SC spacing	1272 SCs / 15 kHz
Nominal transform size ($N_{\text{OFDM},m}$)	2048
Oversampling factor (N_{ov})	4
Modulation	QPSK, 16-/64-/256-QAM
Maximum number of iterations	10, 20

In this evaluation, it is assumed that set $\mathcal{K}_{\mathcal{M}}$ includes two different modulation schemes, meaning that ICWEF filter is created based on the EVM requirements of two different modulation schemes. The obtained results for different sizes of sets $\mathcal{K}_{\mathcal{M}_1}$ and $\mathcal{K}_{\mathcal{M}_2}$ are shown in Fig. 3. Results that are obtained with 10 and 20 iterations are given in subfigures (a) and (b), respectively. It should be noted that in the allocation, it is assumed that sets $\mathcal{K}_{\mathcal{M}_1}$ and $\mathcal{K}_{\mathcal{M}_2}$ represent the bands that tolerate higher and lower clipping noise power, respectively. The ICEF algorithm that is presented in [9] does not constraint the clipping noise level in $\mathcal{K}_{\mathcal{E}}$ and configures some PRBs as $\mathcal{K}_{\mathcal{F}}$. Such a utilization may not be reasonable because of the critical EVM requirements, but performance of this scheme is also given as reference.

According to the results, ICEF algorithm always provides lower PAPR than the case with modulation pair QPSK/256-QAM due to the constraint on clipping noise in $\mathcal{K}_{\mathcal{E}}$. With ICEF, EVM requirements are satisfied for modulations allocated to PRBs in $\mathcal{K}_{\mathcal{F}}$. However, this is not the case with the PRBs included in $\mathcal{K}_{\mathcal{E}}$ as EVM requirements may not be satisfied especially when high amount of

PRBs are configured as $\mathcal{K}_{\mathcal{F}}$. Besides, when whole $\mathcal{K}_{\mathcal{M}_2}$ set is considered as clipping noise-free set, indicated by $\mathcal{K}_{\mathcal{F}}$ in Fig. 3, worse performance than with ICEF is observed, which shows the domination of limiting clipping noise in $\mathcal{K}_{\mathcal{E}}$. This case with $\mathcal{K}_{\mathcal{M}_2} = \mathcal{K}_{\mathcal{F}}$ is a special one because of the exploitation of particular PRBs as clipping noise free PRBs whereas remaining ones are exploited in clipping noise allocation in accordance with the EVM requirements of the modulations. Besides, for a particular range of $\mathcal{K}_{\mathcal{M}_2}$, modulating $\mathcal{K}_{\mathcal{M}_2}$ with 16-QAM and 64-QAM provide better performance when compared to the ICEF algorithm. It is promising that when card($\mathcal{K}_{\mathcal{M}_2}$) is high enough, 7 dB PAPR can be achieved with 72 PRB allocation for 64-QAM, and 6.5 dB PAPR can be achieved with 102 PRB allocation for 16-QAM, assuming that QPSK is used in $\mathcal{K}_{\mathcal{M}_1}$.

These results show that the scheduling decision made by the base station scheduler has a significant impact on the achievable PAPR, and to fully optimize the system throughput, the scheduler should be aware of the impact of decision on the PAPR. For example, it can be noted that all high modulation order users should not be scheduled in the same subframe as the PAPR reduction is more limited in this case. When serving users with lower order modulations, as QPSK or 16-QAM, more aggressive PAPR reduction can be supported and higher average PA output power is also achieved in this case. The ICWEF method can be flexibly configured based on these considerations and desired performance can be obtained in a straightforward manner.

IV. PROPOSED PAPR REDUCTION SOLUTIONS IN MIXED-NUMEROLOGY SYSTEMS

A. MIXED-NUMEROLOGY ICWEF (MN-ICWEF)

One feasible approach to reduce the PAPR in mixed-numerology case is to reduce the PAPR of subband signals separately and then aggregate them to create the mixed-numerology signal. In line with this, we propose MN-ICWEF method which has a straightforward implementation and simple structure. Accordingly, ICWEF method is applied separately for each subband and clipped-and-filtered signals are combined to create the composite mixed-numerology signal.

To this end, first clipping is applied to each subband signal as shown in (6). Then, ICWEF method is applied for each subband signal, which corresponds to realization of (10) and (13)–(16) subsequently. This way, PAPR-reduced subband signal $\mathbf{x}_m^{(\mathcal{L})}$ is obtained for subband m. Then, subband signals (16) are combined with WOLA processing and then summed, which can be expressed as

$$\mathbf{x}^{(\mathcal{L})} = \sum_{m=0}^{M-1} \mathbf{K}_m \mathbf{x}_m^{(\mathcal{L})}. \tag{17}$$

However, this approach—even though being straightforward—has also several drawbacks. Specifically, the PAPR increases due to the aggregation of independent signals and also the MSE requirements may not be fulfilled due to INI. Satisfying the corresponding PAPR requirements for each subband signal is not the optimal choice as it neglects the peaks that emerge from the aggregation of subband signals. Moreover, INI should also be taken into account in the PAPR reduction, as otherwise degradation in both PAPR and MSE is inevitable. These issues will be demonstrated and evaluated later with numerical and measurement results.

B. MN-ICWEF WITH INTER-NUMEROLOGY INTERFERENCE CANCELLATION (MN-ICWEF-INIC)

As already noted, the adoption and realization of mixed-numerology allocations are essential for many different 5G NR use cases but are also problematic as INI emerges due to the aggregation of different subband signals. Since each subband signal is created as a separate CP-OFDM signal, due to CP-OFDM's poor spectral containment performance, undesired spectral emission arises in other BWPs that are allocated for different services or users. Furthermore, existing PAPR reduction methods for single-numerology OFDM cannot be directly applied to mixed-numerology OFDM signals as either PAPR increases when separately PAPR-reduced signals are aggregated or an additional interference emerges due to the PAPR reduction over aggregated multi-numerology signal. Conventional CP-OFDM waveform does not contain any mechanism to prevent these issues and existing PAPR algorithms also do not support mixed-numerology utilization. In line with this, mixed-numerology ICEF method, presented in [11], effectively reduces PAPR in mixed-numerology systems. The mixed-numerology ICEF method includes an INI cancellation mechanism and interference cancellation is realized in the PAPR reduction process, resulting in an effective PAPR reduction for mixed-numerology systems.

In this study, MN-ICWEF-INIC is proposed and MCS specific clipping noise filtering is combined with the mixed-numerology PAPR reduction that is realized with the mixed-numerology ICEF method. Block diagram of the considered TX structure is shown in Fig. 4. In this TX structure, first BWP specific CP-OFDM signals are generated with the corresponding numerology and mixed-numerology signal is obtained after the summation of these subband signals. Then, iterative PAPR reduction method is applied, which starts with the clipping step. After CP removal and conversion of subband signals from time to frequency domain, INI caused by other subband signals on the considered subband is obtained and removed from the sum signal. Separation of the clipping noise and filtering of the clipping noise with MCS-specific ICWEF filter are implemented next. Then, the filtered clipping noise is added back to the original signal. After inverse fast-Fourier-transform (IFFT) and CP addition, clipped-and-filtered mixed-numerology signal is obtained by aggregating the ICWEF processed subband signals. Operation ends when the given maximum number of iterations are completed or PAPR level of the mixed-numerology signal matches the target PAPR level. In the last iteration, WOLA processing can also be implemented depending on the choice and this block is shown with dashed box in Fig. 4. Subband-specific

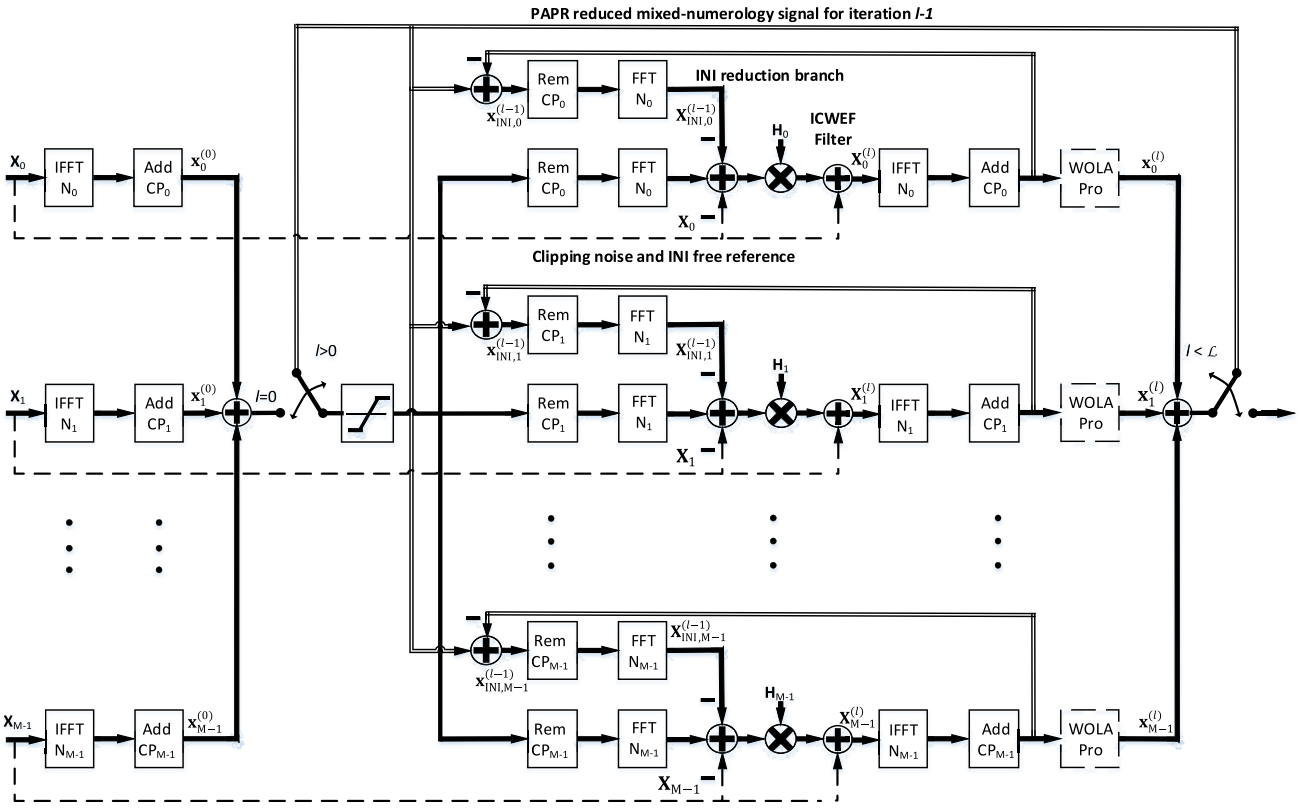

FIGURE 4. Block diagram of the proposed MN-ICWEF-INIC method for mixed-numerology systems.

WOLA processing is required to fulfill the out-of-band emission requirements defined in [24] and used to meet these requirements.

As an important note, the mixed-numerology operation causes non-orthogonality between subband signals which complicates the timing synchronization of individual signals [25]. In order to prevent the degradation of the CP part of the symbol, CP is regenerated in every iteration in MN-ICWEF-INIC method and this way the symbol timing synchronization is guaranteed.

The mathematical formulation of the structure shown in Fig. 4 can be expressed as follows. After generation of the subband signals, the INI component is obtained in time-domain, which can be expressed for subband m as

$$\mathbf{x}_{\mathrm{INI},m}^{(l-1)} = \sum_{\substack{i=0 \\ i\neq m}}^{M-1} \mathbf{x}_i^{(l-1)}. \tag{18}$$

Then, CP-OFDM RX is implemented for each subband and frequency-domain clipping noise is separated after removal of the INI component. This operation can be expressed for k th subcarrier of m th subband as

$$C_{m,s}^{(l)}[k] = \bar{X}_{m,s}^{(l)}[k] - X_{m,s}[k] - X_{\mathrm{INI},m,s}^{(l-1)}[k], \tag{19}$$

where $\bar{X}_{m,s}^{(l)}[k]$ and $X_{\mathrm{INI},m,s}^{(l-1)}[k]$ represent the frequency-domain samples of clipped signal and INI component at k th subcarrier, respectively. It should be noted that clipping noise component presented in (19) is different from (10) due to the existence of INI. Afterwards, clipping noise is filtered by applying ICWEF filter and added back to original signal, which is expressed as

$$X_{m,s}^{(l)}[k] = X_{m,s}[k] + H_{\mathrm{ICWEF},m}^{(l)}[k] C_{m,s}^{(l)}[k]. \tag{20}$$

After IFFT and CP addition, clipped-and-filtered signals are obtained for each subband and with summation, aggregated signal is obtained, which can be denoted as

$$\mathbf{x}^{(l)} = \sum_{m=0}^{M-1} \mathrm{vec}\left(\mathbf{T}_{\mathrm{CP},m} \mathbf{W}_{N_m}^{-1} \mathbf{X}_m^{(l)}\right). \tag{21}$$

When $\mathcal{L}$ iterations are completed or PAPR level of the aggregated signal matches the target level, operation is stopped and WOLA processing is implemented as the last block, resulting in final output signal $\mathbf{x}^{(\mathcal{L})}$.

V. COMPUTATIONAL COMPLEXITY OF THE PROPOSED PAPR REDUCTION METHODS

The basic CP-OFDM TX structure does not include any PAPR reduction mechanism and this structure is not effective in terms of PAPR. However, embedding any additional processing block to CP-OFDM TX structure to improve the PAPR performance brings an increase in computational complexity. Since energy consumption is an important criteria for the communication hardware, increase in computational complexity of the basic CP-OFDM TX structure should be moderate. From this perspective, computational complexity

is a key metric to evaluate the potential of the proposed methods.

In iterative PAPR reduction algorithms, the most computationally complex blocks are DFTs and IDFTs. In practice, these transforms are implemented through the use of FFT and IFFT, and by following the derivations of [26], FFT requires $\mathrm{MUL}_{\mathrm{FFT}}(N_m) = N_m \log_2 N_m - 3N_m + 4$ real multiplications and $\mathrm{ADD}_{\mathrm{FFT}}(N_m) = 3N_m \log_2 N_m - 3N_m + 4$ real additions. In CP-OFDM TX processing, one IFFT operation brings $\mathrm{MUL}_{\mathrm{FFT}}(N_m)$ real multiplications and $\mathrm{ADD}_{\mathrm{FFT}}(N_m)$ real additions for each symbol. In ICF case, as mentioned in [9], each iteration can be realized with one FFT and one IFFT, causing $2\,\mathrm{MUL}_{\mathrm{FFT}}(N_m)$ real multiplications and $2\,\mathrm{ADD}_{\mathrm{FFT}}(N_m)$ real additions. WOLA processing also requires round $4(0.7N_{\mathrm{CP},m})$ real multiplications and $2(0.7N_{\mathrm{CP},m})$ real additions per symbol. It should also be reminded that WOLA processing is applied only in the last iteration. In total, number of real multiplications that are required for realization of ICF method for S symbols is equal to

$$\mathrm{MUL}_{\mathrm{ICF}} = (2S\mathcal{L} + S)\,\mathrm{MUL}_{\mathrm{FFT}}(N_m) + 2.8SN_{\mathrm{CP},m}, \quad (22)$$

and total number of additions is equal to

$$\mathrm{ADD}_{\mathrm{ICF}} = (2S\mathcal{L} + S)\,\mathrm{ADD}_{\mathrm{FFT}}(N_m) + 1.4(S-1)N_{\mathrm{CP},m}. \quad (23)$$

Due to the specific filtering operation and separation of clipping noise from clipped signal in frequency domain, ICWEF requires one additional complex multiplication and two additional complex additions, which result in $2S\mathcal{L}N_m$ extra real multiplications and $4S\mathcal{L}N_m$ extra real additions when compared to the ICF method, i.e.,

$$\mathrm{MUL}_{\mathrm{ICWEF}} = \mathrm{MUL}_{\mathrm{ICF}} + 2S\mathcal{L}N_m, \quad (24)$$

$$\mathrm{ADD}_{\mathrm{ICWEF}} = \mathrm{ADD}_{\mathrm{ICF}} + 4S\mathcal{L}N_m. \quad (25)$$

In mixed-numerology cases, computational complexity increases due to the existence of separate BWPs. In MN-ICWEF case, total number of multiplications required is equal to

$$\mathrm{MUL}_{\text{MN-ICWEF}} = \sum_{m=0}^{M-1}\big((2S_m\mathcal{L} + S_m)\,\mathrm{MUL}_{\mathrm{FFT}}(N_m) + 2.8S_mN_{\mathrm{CP},m} + 2S_m\mathcal{L}N_m\big), \quad (26)$$

and the total number of additions required is equal to

$$\mathrm{ADD}_{\text{MN-ICWEF}} = \sum_{m=0}^{M-1}\big((2S_m\mathcal{L} + S_m)\,\mathrm{ADD}_{\mathrm{FFT}}(N_m) + 1.4(S_m-1)N_{\mathrm{CP},m} + 4S_m\mathcal{L}N_m\big) + 2(M-1)S_0N_{\mathrm{WOLA},0}, \quad (27)$$

where last term of the equation that is not included in summation part, represents the combination of separately PAPR-reduced WOLA processed BWPs. It can be seen that except this last term, (26) and (27) are quite similar to (24) and (25), and MN-ICWEF equations are basically containing summation of the multiplications and additions required for the implementation of ICWEF for each BWP, resulting in total computational complexity that is associated with M BWPs.

The MN-ICWEF-INIC method has higher computational complexity than MN-ICWEF because of the more evolved mixed-numerology related INI and PAPR reduction mechanism. Beside the blocks that are included also in MN-ICWEF structure which are CP-OFDM processing, ICWEF-based PAPR reduction, WOLA processing and mixed-numerology signal creation blocks; INI and PAPR reduction mechanisms bring four additional blocks that increase the complexity. The INI reduction block is one of these blocks and requires both multiplications and additions, namely

$$\mathrm{MUL}_{\mathrm{INIC}} = \sum_{m=0}^{M-1} S_m\mathcal{L}\,\mathrm{MUL}_{\mathrm{FFT}}(N_m), \quad (28)$$

$$\mathrm{ADD}_{\mathrm{INIC}} = \sum_{m=0}^{M-1} S_m\mathcal{L}\big(\mathrm{ADD}_{\mathrm{FFT}}(N_m) + 2N_m + 2\big(N_m + N_{\mathrm{CP},m}\big)\big). \quad (29)$$

Other three blocks are combining separate BWP signals before MN-ICWEF-INIC as in (3), combining PAPR-reduced BWP signals at the end of each MN-ICWEF-INIC iteration as in (21), and combining PAPR-reduced and WOLA-applied BWP signals. These blocks only require additions and the number of multiplications does not increase. Number of real additions that are required for implementing these three separate combination blocks can be expressed in respective order as

$$\mathrm{ADD}_{\mathrm{COM},1} = 2(M-1)S_0\big(N_0 + N_{\mathrm{CP},0}\big), \quad (30)$$

$$\mathrm{ADD}_{\mathrm{COM},2} = (\mathcal{L}-1)\,\mathrm{ADD}_{\mathrm{COM},1}, \quad (31)$$

$$\mathrm{ADD}_{\mathrm{COM},3} = 2(M-1)S_0N_{\mathrm{WOLA},0}. \quad (32)$$

Overall, the total number of real multiplications for the MN-ICWEF-INIC implementation can be straightforwardly represented as

$$\mathrm{MUL}_{\text{MN-ICWEF-INIC}} = \mathrm{MUL}_{\text{MN-ICWEF}} + \mathrm{MUL}_{\mathrm{INIC}}. \quad (33)$$

In addition, total number of real additions required for implementation of MN-ICWEF-INIC can be noted as

$$\mathrm{ADD}_{\text{MN-ICWEF-INIC}} = \mathrm{ADD}_{\text{MN-ICWEF}} + \mathrm{ADD}_{\mathrm{INIC}} + \mathrm{ADD}_{\mathrm{COM}}, \quad (34)$$

where $\mathrm{ADD}_{\mathrm{COM}} = \mathrm{ADD}_{\mathrm{COM},1} + \mathrm{ADD}_{\mathrm{COM},2} + \mathrm{ADD}_{\mathrm{COM},3}$. These combinations also increase the complexity, but the increase corresponds to only 3% of the additions necessary for the INI reduction step. Therefore, we can claim that the main difference between MN-ICWEF and MN-ICWEF-INIC methods in terms of the complexity is the INI reduction mechanism included in MN-ICWEF-INIC.

Numerical comparison of computational complexity for all methods is provided in Table 2. These results are obtained by

TABLE 2. Total number of real multiplications (mult.) and additions required for realization of different methods using 20 iterations.

Method	Mult. (Per Iter)	Additions (Per Iter)	Mult. (Total)	Additions (Total)
ICF	6.1×10^8	2.2×10^9	1.3×10^{10}	4.5×10^{10}
ICWEF	6.8×10^8	2.4×10^9	1.4×10^{10}	4.8×10^{10}
MN-ICWEF	2.4×10^9	4.6×10^9	2.6×10^{10}	9.2×10^{10}
MN-ICWEF-INIC	5.6×10^9	7.0×10^9	3.8×10^{10}	1.4×10^{11}

utilizing the parameters given in Table 3, where 20 iterations are run for all methods. Accordingly, ICWEF method has approximately 11% increase in real multiplications and 6% additional real additions with respect to ICF, which can be seen as moderate increases. In MN-ICWEF case, number of real multiplications and real additions increase by 111% and 103%, respectively. These results are reasonable because two BWP signals whose parameters can be seen from Table 3, are separately processed. Therefore, approximately two times increase in complexity is an expected result

On the other hand, MN-ICWEF-INIC method increases the number of multiplications and additions approximately by factor of three when compared to the ICF processing. Computational complexity of MN-ICWEF-INIC is approximately 1.5 times higher than that of MN-ICWEF, and this difference implies the cost of implementing INI reduction. The MN-ICWEF-INIC method increases the implementation complexity by 3.7×10^{10} real multiplications and 14.1×10^{10} real additions when compared with the original mixed-numerology waveform processing assuming that 20 iterations are needed for the processing. But this increase in the computational complexity is acceptable because it increases the achievable transmission power significantly, as it will be shown with the experimental results. Since PA consumes most of the power in transmitter chain, the obtained improvement on the PA power consumption is more significant than the degradation in computational complexity.

VI. SDR TESTBED AND 5G NR EMISSION REQUIREMENTS

A. SDR PROTOTYPE SYSTEM AND MEASUREMENT SETUP

An SDR testbed is created and developed to quantify the performance of the proposed PAPR reduction methods with measurements and validate the performance advantages that are observed with simulation results. Block diagram and actual photo of the testbed are shown in Fig. 5. In our experiments, the focus is on downlink, i.e., the 5G NR base-station transmitter system. As the first step, the baseband signal is generated on the host processor and generated data is transferred to the Vector Signal Transceiver (VST) device via PCIe connection. In this implementation, base station functionality is realized by using the NI PXIe-5840 VST device, which supports instantaneous bandwidth up to 1 GHz and carrier frequency range of 9 kHz to 3.5 GHz[27]. Moreover, this device also realizes

TABLE 3. The main parameters that are used in the simulations and experiments whose results are shown in Section VII.

Parameter	Value
Common parameters for all methods	
PRB size	12 subcarriers
Oversampling factor (N_{ov}) (for simulations)	4
Maximum number of iterations	20
WOLA: Nominal window length ($N_{\text{WOLA},m}$)	$1.7N_{\text{CP},m} + N_{\text{OFDM},m}$
Modulation set ($\mathcal{K}_{\mathcal{M}}$) (unity with ICF)	QPSK, 16-/64-/256-QAM
Number of simulated ICWEF masks	100
Target PAPR levels	3 dB to 9 dB
ICF / ICWEF	
Number of subbands (M)	1
SCS	30 kHz
Number of PRBs / active SCs ($N_{\text{act},m}$)	51 / 612
Nominal transform size ($N_{\text{OFDM},m}$)	1024
Number of transmitted OFDM symbols (S_m)	2048
MN-ICWEF / MN-ICWEF-INIC	
Number of subbands (M)	2
SCS for BWP_m, $m \in \{0, 1\}$	{30, 60} kHz
Number of PRBs / active SCs ($N_{\text{act},m}$)	{24, 11} / {288, 132}
Nominal OFDM transform size ($N_{\text{OFDM},m}$)	{512, 256}
Number of transmitted OFDM symbols (S_m)	{2048, 4096}
Experiment Parameters	
Carrier frequency	1.84 GHz
5G NR DL ACLR limit	45 dB
Gain of ZFL-2500VH+	25 dB
Gain of DL PA	40-50 dB
Oversampling factor (N_{ov}) DPD / experiments	8 / 6
Target PAPR levels	{5, 6, 7}
Number of symbols per subframe for BWP_m	{14, 28}
Ratio of data to pilot symbols for BWP_m	{13, 27}

RF modulation and the pre-amplification operations in the implementation.

The output of the VST device is connected to the driver PA, which is used to increase the power of the signal to the required input power level of the HPA. In order to achieve this functionality, ZFL-2500VH+ PA that can provide a gain level up to 25 dB with output power level of +25 dBm at 1-dB compression point in the operating carrier frequency of 1.84 GHz [28], is used. The output of the driver PA is then transmitted to the HPA, that can provide gain level in the range of 40-50 dB with a third-order output intercept point (OIP3) of +57.3 dBm in the operating carrier frequency of 1.84 GHz. At the output of HPA, three attenuators that provide a total attenuation value of 60 dB are used. In this way, high power level of the output of the HPA is reduced to the required level for the used measurement RX.

The NI PXIe-5840 VST is a high-quality instrument supporting high sampling rates. It is thus used as the measurement RX for the evaluation of the 5G NR OOB emissions and NR ACLR. On the host PC, RX-side baseband processing is realized and, EVM as well as ACLR are measured. In

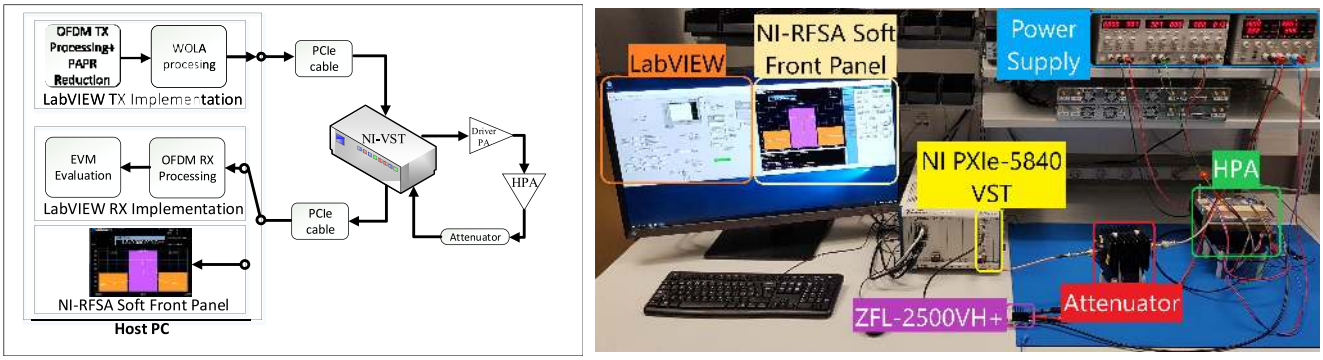

(a) Basic block-diagram

(b) Real hardware setup in the laboratory

FIGURE 5. Illustration of the developed SDR prototype and the overall RF measurement system.

this process, LabVIEW and NI RFSA Soft Panel are used as the software tools by utilizing the corresponding hardware and communications libraries. It should be noted that realization of separate RXs in MN-ICWEF-INIC case is achieved by using NI PXIe-5840 VST simultaneously, running separate codes thanks to device's advanced hardware capabilities. Moreover, since corresponding 5G NR OOB emission limits are more strict in DL transmission case, WOLA processing is applied after generation of PAPR reduced signals. In this way, OFDM's poor OOB emission performance is improved. In addition, DPD operation is also applied to maximize the PA efficiency and also the transmission power level.

B. 5G NR PHYSICAL LAYER FRAME STRUCTURE

Guidelines for the configuration of 5G NR physical layer frame structure are given in [29]. Accordingly, uplink (UL), downlink (DL) and sidelink transmissions are organized into frames and each frame corresponds to duration of 10 ms. Moreover, each frame contains 10 subframes with each of them containing 14 OFDM symbols. The number of OFDM symbols contained in each subframe changes based on the configured subcarrier spacing (SCS). Since SCS cases of 30 kHz and 60 kHz are used in the testbed, each subframe is configured to contain two and four slots (28 and 56 OFDM symbols, respectively) for each numerology, based on the details given in [29, Table 4.3.2-1]. Moreover, extended CP is configured for the first OFDM symbol of every half subframe and normal CP is configured for the other symbols.

In order to obtain an accurate channel estimation, pilot OFDM symbols are inserted and every first OFDM symbol of each half subframe is configured as the pilot symbol. Pilot symbols are generated by following the details on the generation of pseudo-random sequence given in [29], and each pilot is configured as length-31 Gold sequence. First symbol of each subframe is generated with the same index of Gold sequence and these are used in the estimation of timing offset and CFO. In the estimation of timing offset and CFO, correlation between the known pilot symbol and received signal is computed in time domain and based on the result, timing offset and CFO are estimated. In the channel estimation phase, received pilot symbols are transformed to frequency domain and channel coefficients are obtained by using zero-forcing and filtering. Then, one-dimensional interpolation is applied to obtained coefficients and channel estimation is achieved.

C. 5G NR TRANSMITTER RF EMISSION REQUIREMENTS

The 5G NR ACLR is the ratio between filtered mean power of the operating NR channel and the filtered mean power of an adjacent NR channel [24]. Accordingly, the filtered mean power of the operating NR channel is computed with a square filter of bandwidth equal to the configuration bandwidth of the transmitted signal that is centered on the allocated channel frequency [24]. Similarly, filtered mean power of an adjacent NR channel is computed with a square filtered that is centered on the adjacent channel frequency. In the evaluation of ACLR, details given in [24, Table 6.6.3.2-1] are followed, and channel bandwidth of 20 MHz and BS ACLR limit of 45 dB are considered.

The 5G NR OOB spectrum emission mask for BSs operating in FR1 is defined in [30]. f_{offset} represents the separation between the channel edge frequency and the centre of the measuring filter [30]. There are five different regions included in the spectrum emission mask, changing based on the value of f_{offset}. For first three cases, the measurement filter bandwidth of 30 kHz is used and for the other two cases, the measurement filter bandwidth of 1 MHz is defined. For the intervals of 0.015 MHz $\leq f_{\text{offset}} <$ 0.215 MHz, 0.215 MHz $\leq f_{\text{offset}} <$ 1.015 MHz, and 1.015 MHz $\leq f_{\text{offset}} <$ 1.5 MHz, the spectrum emission limit is equal to -12.5 dBm, -12.5 dBm $-15(\frac{f_{\text{offset}}}{10^6} - 0.215)$ dB, and -24.5 dBm, respectively. For the other two intervals which are 1.5 MHz $\leq f_{\text{offset}} <$ 10.5 MHz and 10.5 MHz $\leq f_{\text{offset}}$, the spectrum emission limit is equal to -11.5 dBm and -15 dBm, respectively. Other details of the definitions can be seen in [30, Table 6.6.4.5.3.2-1].

D. DPD IMPLEMENTATION

In order to maximize the DL transmit power, the HPA is operated very close to its saturation point, delivering up to

+50 dBm TX power. As a consequence, the PA will introduce a significant amount of nonlinear distortion that will result in a violation of the EVM and ACLR specifications. In order to ensure maximum power transmission while meeting the signal quality metrics, a DPD-based linearizer is implemented [20].

The DPD is based on the closed-loop architecture and on the injection principle [31], where the DPD injects to the PA input a low power nonlinear signal with similar structure to the nonlinear distortion introduced by the PA but with opposite phase, so that the distortion at the PA output is minimized. Memory polynomial basis functions (BFs) [20] are considered as the regressors of the DPD. For parameter learning, a block least-means-squares (LMS) learning rule is adopted [20], [31]. As the BFs are strongly mutually correlated, the self-orthogonalized version of the LMS rule is adopted [20], [31], so that a faster and smooth convergence is achieved.

This specific DPD solution is considered because it entails very low complexity compared to widely adopted techniques such as the indirect learning architecture (ILA) based on least-squares (LS) fitting for parameter learning, enabling thus its real-time implementation. A detailed description of the implemented algorithm and its comparison against the LS-based ILA solution, also in terms of complexity, can be found in [31]. The adopted parameterization is as follows: the nonlinearity order and the memory depth of the DPD filter are set to 9 and 3, respectively. The block LMS learning algorithm employs 15 block iterations, each of them employing 20.000 samples and is executed only once at the beginning of the data transmission.

VII. SIMULATION AND MEASUREMENT RESULTS

A. SIMULATION RESULTS

The performance of ICF, ICWEF, and MN-ICWEF-INIC is evaluated with simulations. In the evaluation, PAPR is measured by computing the sample-wise CCDF of PAPR and 20 MHz NR channel configuration is implemented by using the parameters that are shown in Table 3. In the ICWEF case, 51 PRBs are used with the configured SCS value. Since 51 PRBs cannot be equally divided by four which is the number of different modulations used, 12 PRBs are modulated with three different modulations and remaining 15 PRBs are modulated with the fourth modulation. The modulations are randomly selected and 100 different masks are evaluated for the proposed methods. In the mixed-numerology case, as shown in Table 3, two BWPs are configured and each one is configured as 10 MHz channel with SCSs of 30 and 60 kHz, respectively. Following structure is implemented in the generation of 100 random masks. First BWP is equally divided between two different modulations and since 11 PRBs are included in the second BWP, it is divided as 5 PRBs and 6 PRBs between two different modulations. Indices and modulations are randomly selected, and 100 different masks are generated by following this structure.

Firstly, PAPR distributions are evaluated for target PAPR level of 6 dB and results are shown in Fig. 6 (a). Here, PAPR distribution of original mixed-numerology waveform is also given as a reference. Since both subband signals are relatively long signals due to the corresponding configuration, a distribution very close to that of mixed-numerology waveform, is obtained for both BWPs. Therefore, the PAPR distributions for these subband signal are omitted from Fig. 6(a).

It can be seen that both methods meet the target PAPR level at CCDF probability level of 1%. Effective PAPR reduction mechanism in the MN-ICWEF-INIC method provides a quite good PAPR performance, but performance starts to degrade after CCDF probability level of 0.1% and starts to diverge from than that of the other two methods, due to the misalignment of CP samples in the PAPR reduction. On the other hand, ICWEF provides almost same performance as that of ICF, with a minor difference at CCDF probability level of 0.01%. One main reason of this is the limitation of MSE with ICWEF filter, as this causes some degradation in PAPR performance, but at relatively low CCDF probability levels. Otherwise, it provides an effective PAPR performance.

As the second evaluation, the achieved PAPR levels at CCDF probability level of 1% for different target PAPR levels are evaluated and shown in Fig. 6 (b). It is clear that ICF achieves the ideal performance, as all target PAPR levels are met. On the other hand, ICWEF and MN-ICWEF-INIC meet the target PAPR levels for the interval of 6 dB to 9 dB. However, degradation appears for lower target PAPR levels, which can be explained with ICWEF filtering and mixed-numerology interference. When CCDF probability level of 1% is considered, quite promising PAPR performance can be obtained with the MN-ICWEF-INIC, and it can provide almost same performance as that of ICWEF. Overall, both methods are quite effective, they provide same PAPR performance as ICF, down to target PAPR level of 6 dB.

As the final evaluation, MSE performance is measured and obtained results are given in Fig. 6 (c). Here, results are given separately for each modulation. It can be seen that both ICWEF and MN-ICWEF-INIC meet the individual MSE requirements of the modulations and ICF violates the requirements, except for relatively high target PAPR levels. Another interesting observation is the saturation in MSE performance when target PAPR levels less than 6 dB are targeted, which demonstrates that high clipping noise power is required to meet such target PAPR levels.

Due to the MSE requirements of the modulations, higher clipping noise power cannot be supported and this translates into degradation in PAPR performance. The minimum achievable PAPR level is limited by the MSE requirements and, for the proposed methods, 5.0 dB level can be achieved. ICF, despite its effective PAPR reduction capability, can achieve only 7.7 dB as target levels higher than this level result in violation of 256-QAM MSE requirement. Overall, results that are shown in Fig. 6 prove the effectiveness of the ICWEF and MN-ICWEF-INIC, and good PAPR

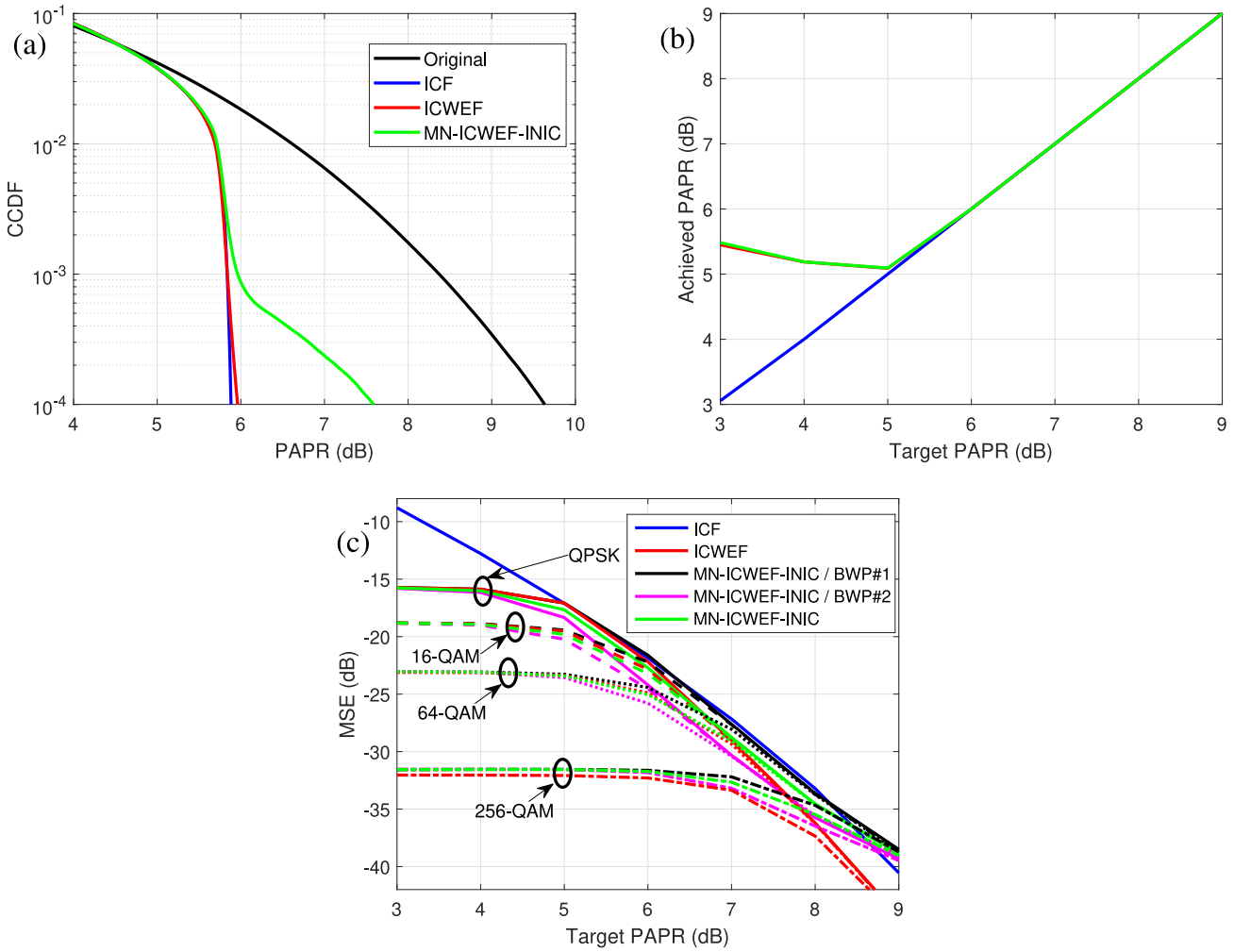

FIGURE 6. PAPR and MSE results for different PAPR reduction methods. PAPR distributions are shown in (a) for PAPR target level of 6 dB. Moreover, obtained PAPR results at CCDF probability level of 1% and achieved modulation-specific MSE performance results are shown for different target levels in (b) and in (c), respectively.

performance can be obtained without violating individual MSE requirements.

B. SDR PROTOTYPE MEASUREMENT RESULTS

In the experiments, both the single-numerology and mixed-numerology operations are considered and different methods including ICF, MN-ICWEF, MN-ICWEF-INIC with different masks are tested. The WOLA and DPD operations are also applied to all considered methods. Moreover, PAPR, ACLR, 5G NR DL spectrum emission mask and EVM are considered as the main performance metrics. Based on these, the maximum achievable transmission power level for each method is measured with the best possible configuration that does not result in violation of the performance metrics. Measurements are conducted based on the parameters that are shown in Table 3, and 5G NR channel of 20 MHz is considered with SCS cases of 30 kHz and 60 kHz. As modulations and EVM limits, four modulation schemes which are QPSK, 16-QAM, 64-QAM and 256-QAM, are utilized with an EVM margin of 1%, to compensate the additional error that is caused by hardware nonlinearities. As it will be shown, this margin is sufficient to satisfy the RX-side EVM requirements.

In order to stabilize the operation point of PA and DPD operation, an additional clipping operation is applied after the MN-ICWEF or MN-ICWEF-INIC based PAPR reduction to guarantee that PAPR level is under the required threshold. However, the misalignment between CP samples in MN-ICWEF-INIC method and imperfections in MN-ICWEF method might result in relatively high PAPR values and if PAPR reduced signal is clipped to a level such as 6 dB, OOB emissions increase. In this case, satisfying the ACLR limit becomes impossible because last clipping stage already degrades the ACLR level of 45 dB, and DPD operation becomes useless. Therefore, low PAPR levels such as 3 dB cannot provide the desired performance and target PAPR level of the methods is limited because of the mentioned difficulty.

1) SINGLE-NUMEROLOGY PERFORMANCE COMPARISON OF ICF AND ICWEF

In order to test the performance of ICWEF method, different methods including original WOLA-processed CP-OFDM

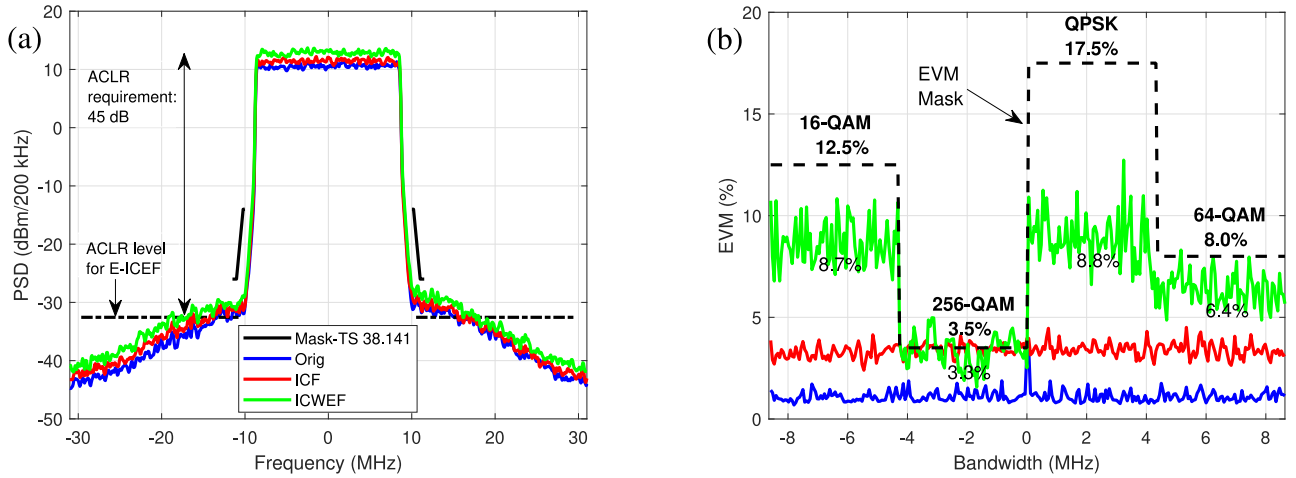

FIGURE 7. Measured PSD responses in the SDR prototype system with respect to spectrum emission mask, in (a), and the corresponding subcarrier-wise EVM results, in (b). Single-numerology scenario where the BWP is configured as 20 MHz 5G NR channel with SCS of 60 kHz. In (a), ACLR limit with respect to passband power level of ICWEF is shown with dash-dot line. Corresponding EVM limits for the utilized modulations are also shown with dashed line in (b).

signal, ICF and ICWEF are tested and obtained results are shown in Fig. 7. In the experiments, only one ICWEF mask is considered. The obtained PSD responses for the methods are presented in Fig. 7 (a) with 5G NR DL spectrum emission mask and 5G NR DL ACLR limit with respect to the passband power level of ICWEF method. The advantage of ICWEF method is visible as a higher transmission power level than the other two cases can be obtained. When compared to the ICF case, 1.4 dB higher transmission level can be obtained with ICWEF and, difference is around 3.1 dB when it is compared with the original waveform. It can also be seen from Fig. 7 (a) that some samples of the PSD responses exceed the ACLR limit occasionally in the OOB region, but the average power in OOB regions is still below the ACLR limit of 45 dB.

The measured RX-side EVM results are presented in Fig. 7(b), where EVM mask visualising the used ICWEF mask, is also shown with dashed line to show the reference values for the utilized modulations. Accordingly, original waveform provides a really good EVM performance as it achieves a limited transmission power and it is affected less from the PA nonlinearities. It should be noted that the original waveform has quite good EVM performance but PAPR performance and related ACLR limit are the main limitations thereof. Therefore, PA degradation caused by high PAPR limits the achievable transmission power level. In ICF case, EVM values are more or less same for all subcarriers and the average EVM value satisfies the EVM requirement of highest order modulation, which is 256-QAM. In this case, 256-QAM limits the transmission power and PAPR levels less than 7 dB cannot be targeted because of the EVM limit.

On the other hand, a PAPR target down to 6.2 dB can be targeted with ICWEF as it achieves a better PAPR performance thanks to the more effective clipping noise allocation. As the reference, EVM limits are given with bold font above the EVM mask and the measured average EVM values for each region of ICWEF are given below the EVM mask. Accordingly, in the case of 256-QAM modulation, EVM limit is achieved without any more room for the degradation. On the other hand, clear gaps can be seen for QPSK and 16-QAM modulations, where extra 8.7% EVM can be allocated to the QPSK band. However, 256-QAM limits this functionality and these levels cannot be improved with this approach. It is clear that ICWEF is a better choice for single-numerology case and even better gains can be obtained depending on the used EVM mask.

2) MIXED-NUMEROLOGY PERFORMANCE COMPARISON OF MN-ICWEF AND MN-ICWEF-INIC

As the first set of measurement results for the mixed-numerology operation, results for the comparison between original WOLA processed CP-OFDM signal, MN-ICWEF and MN-ICWEF-INIC methods are presented in Fig. 8. Here, target PAPR level of 6 dB is considered and only one ICWEF mask is considered. PSD responses for the methods are given in Fig. 8 (a) with 5G NR DL spectrum emission mask and 5G NR DL ACLR limit with respect to the passband power level of MN-ICWEF-INIC method. Due to the effectiveness of MN-ICWEF-INIC based PAPR reduction, a significantly higher transmission power level is obtained with MN-ICWEF-INIC method when compared to the other two cases. Accordingly, MN-ICWEF-INIC method provides 4 dB higher transmission power level than that of MN-ICWEF method, and advantage of MN-ICWEF over original waveform is quite limited, where difference in power level is only 0.25 dB. To show the effect of DPD operation, a reference case that corresponds to MN-ICWEF-INIC without DPD is also shown in Fig. 8 (a). It is clear that if DPD is not implemented, required ACLR level cannot be satisfied. Moreover, when compared to the MN-ICWEF-INIC with DPD case, this case results in higher transmission power

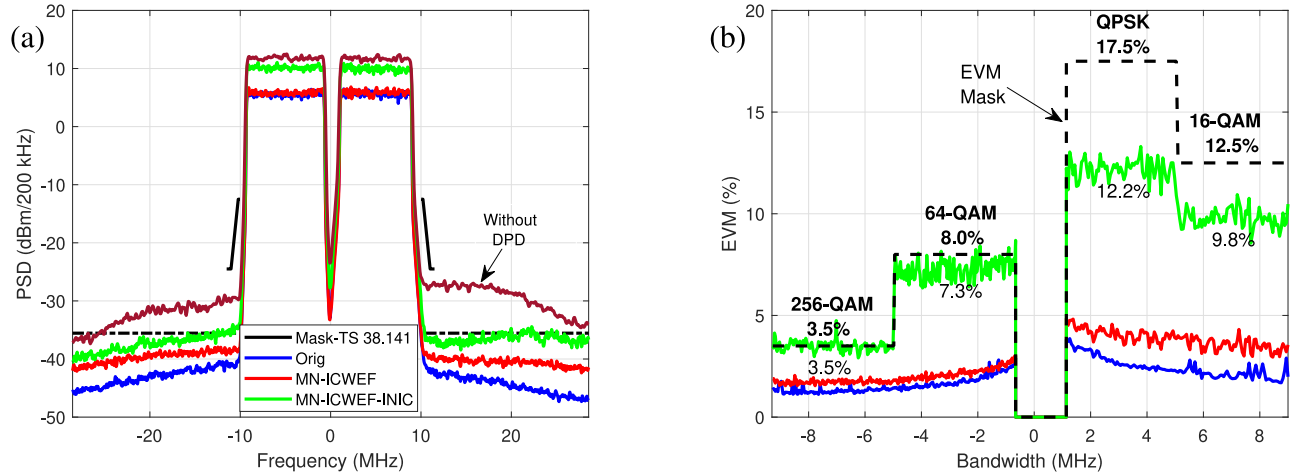

FIGURE 8. Measured PSD responses in the SDR prototype system with respect to spectrum emission mask, in (a), and the corresponding subcarrier-wise EVM results, in (b). Mixed-numerology scenario where the two BWPs are configured as 10 MHz 5G NR channels with SCS values of 30 kHz and 60 kHz, respectively. In (a), first half of the active band corresponds to SCS of 60 kHz and second half represents the 30 kHz case. For reference, the PSD response without DPD is also shown in (a). Corresponding EVM limits for the utilized modulations are additionally shown with dashed line in (b).

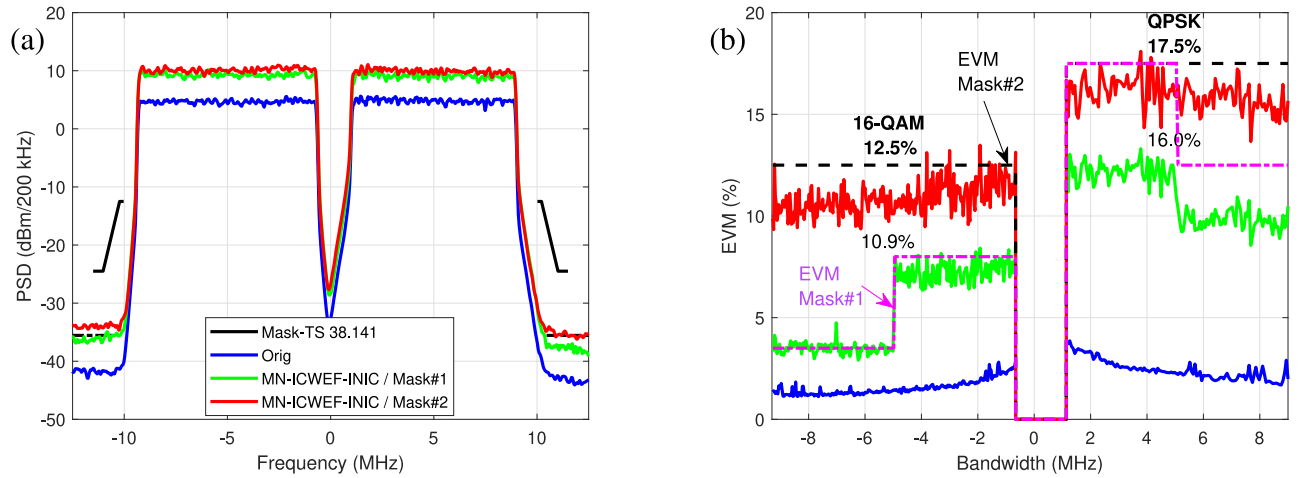

FIGURE 9. Measured PSD responses in the SDR prototype system with respect to spectrum emission mask, in (a), and the corresponding subcarrier-wise EVM results, in (b), for mixed-numerology MN-ICWEF-INIC with two different masks. The two BWPs are configured as 10 MHz 5G NR channels with SCS values of 30 kHz and 60 kHz, respectively. In (a), first half of the active band corresponds to SCS of 60 kHz and second half represents the 30 kHz case. Corresponding EVM limits for the utilized modulations are also shown with dash-dotted and dashed lines in (b).

but as a known fact, DPD operation decreases the transmission power slightly, otherwise, it is quite effective and a quite high transmission power can be obtained without violating the ACLR requirements.

Measured RX-side EVM results are also shown in Fig. 8(b), where used EVM mask is also shown with a dashed line. It is clear that the original signal has quite good EVM performance, where only hardware impairments and mixed-numerology interference affect the EVM performance slightly. In MN-ICWEF case, performance is also similar to the original case because PAPR reduction is not effective and therefore degradation because of the clipping is quite limited. On the other hand, it is clear that EVM performance of MN-ICWEF-INIC is at the edge of the EVM limits especially for 64-QAM and 256-QAM modulations. EVM values confirm the observation and, EVM requirements of 64-QAM and 256-QAM modulations are satisfied without any more room for additional degradation. On the contrary, EVM requirements of QPSK and 16-QAM modulations are satisfied with a reasonably high gap between the achieved results and EVM limits.

3) PERFORMANCE RESULTS FOR MN-ICWEF-INIC WITH TWO DIFFERENT PAPR TARGETS AND CORRESPONDING EVM MASKS

In the second measurement case for mixed-numerology operation, to understand the effect of chosen ICWEF mask, two different cases of MN-ICWEF-INIC with different masks are evaluated and obtained results are given in Fig. 9. In the figures, original waveform is also given as a reference and the first MN-ICWEF-INIC case represents the case with mask that is presented in the previous measurement case. In the second MN-ICWEF-INIC case, only QPSK and 16-QAM modulations are used and, BWPs that are using SCS

of 30 kHz and 60 kHz are modulated with 16-QAM and QPSK, respectively. This type of allocation enables targeting a lower PAPR level than the previous measurement case because of the higher EVM limits, therefore, target PAPR level of 5 dB is considered with this case.

PSD responses together with 5G NR DL spectrum emission mask and 5G NR DL ACLR limit, are shown in Fig. 9(a). When compared to the span of Fig. 8 (a), a narrower span is shown because transmission power levels are quite close for MN-ICWEF-INIC cases and, in this way, performance results can be distinguished from each other. Because of this narrower span, ACLR limit is not clearly visible and it can be thought that second MN-ICWEF-INIC case violates the ACLR limit due to samples with higher power levels in the near edge regions of the channel. However, samples on the farther indices to the channel edges have lower power levels and they decrease the average level below to ACLR limit. Besides this, second MN-ICWEF-INIC case provides 0.85 dB higher power level than that of the first case, and it is approximately 5.30 dB higher than that of the original waveform. Therefore, as expected, easiness in the allocation of clipping noise results in higher transmission power level.

Besides the spectrum evaluation, measured RX-side EVM results are also shown in Fig. 9 (b). In this case, two different EVM masks are shown and, both EVM limits and measured values for the second MN-ICWEF-INIC case are shown with bold and normal font, respectively. When compared to the results in Fig. 8 (b), it can be seen that clipping noise allocation is effectively done also for the higher-order modulations and EVM limit is efficiently exploited. Here, the gap between EVM mask and measured EVM value is obtained as 1.5% and 1.6% for QPSK and 16-QAM, respectively. Overall, it is clear that the utilized ICWEF mask is the key for the performance and depending on the choice, a higher transmission power level can be obtained without violating the corresponding 5G NR performance metrics.

VIII. CONCLUSION

In this article, the transmit signal PAPR reduction problem was addressed in the 5G NR network context, covering both the single-numerology and the mixed-numerology CP-OFDM cases. Firstly, with emphasis on single-numerology networks, the so-called ICWEF method building on frequency-selective PAPR reduction approach was proposed, and implementation details as well as comprehensive performance results were shown and provided. As the most important benefit of the method compared to the state-of-the-art, modulation-specific passband EVM requirements can be flexibly realized and achieved while at the same time facilitating efficient PAPR reduction capabilities. Secondly, the extension to mixed-numerology networks was addressed. To this end, the MN-ICWEF method building on the adoption of the ICWEF processing separately for the different bandwidth parts of subbands was formulated. However, the INI caused by the aggregation of subband signals was shown to be a limiting factor in such approach, and thus a more advanced MN-ICWEF-INIC method was described and proposed where the INI is explicitly considered and cancelled along the iterative PAPR reduction procedure. As demonstrated through the numerical results, very efficient PAPR reduction can be obtained through such approach in mixed-numerology networks. As the ultimate contribution, the performance of the presented methods was also assessed and measured by the developed SDR-based testbed, with the obtained results validating the effectiveness of the proposed solutions. As shown through the vast collection of simulated and testbed-based measured results, the proposed PAPR reduction solutions outperform the state-of-the-art, while being able to provide significant performance gains in the 5G NR networks.

REFERENCES

[1] E. Dahlman, S. Parkvall, and J. Sköld, *5G NR: The Next Generation Wireless Access Technology*. London, U.K.: Academic, 2018.

[2] *New Radio (NR); Overall Description; Stage-2, Technical Specification Group Radio Access Network, Rel. 15*, 3GPP Standard TS 38.300, Jun. 2018.

[3] J. Armstrong, "Peak-to-average power reduction for OFDM by repeated clipping and frequency domain filtering," *Electron. Lett.*, vol. 38, no. 5, pp. 246–247, Feb. 2002.

[4] R. W. Bauml, R. F. H. Fischer, and J. B. Huber, "Reducing the peak-to-average power ratio of multicarrier modulation by selected mapping," *Electron. Lett.*, vol. 32, no. 22, pp. 2056–2057, Oct. 1996.

[5] J. Hou, J. Ge, and F. Gong, "Tone reservation technique based on peak-windowing residual noise for PAPR reduction in OFDM systems," *IEEE Trans. Veh. Technol.*, vol. 64, no. 11, pp. 5373–5378, Nov. 2015.

[6] S. H. Muller and J. B. Huber, "OFDM with reduced peak-to-average power ratio by optimum combination of partial transmit sequences," *Electron. Lett.*, vol. 33, no. 5, pp. 368–369, Feb. 1997.

[7] Y. Rahmatallah and S. Mohan, "Peak-to-average power ratio reduction in OFDM systems: A survey and taxonomy," *IEEE Commun. Surveys Tuts.*, vol. 15, no. 4, pp. 1567–1592, 4th Quart., 2013.

[8] H. Chen and A. M. Haimovich, "Iterative estimation and cancellation of clipping noise for OFDM signals," *IEEE Commun. Lett.*, vol. 7, no. 7, pp. 305–307, Jul. 2003.

[9] S. Gökceli, T. Levanen, T. Riihonen, M. Renfors, and M. Valkama, "Frequency-selective PAPR reduction for OFDM," *IEEE Trans. Veh. Technol.*, vol. 68, no. 6, pp. 6167–6171, Jun. 2019.

[10] X. Zhang, L. Zhang, P. Xiao, D. Ma, J. Wei, and Y. Xin, "Mixed numerologies interference analysis and inter-numerology interference cancellation for windowed OFDM systems," *IEEE Trans. Veh. Technol.*, vol. 67, no. 8, pp. 7047–7061, Aug. 2018.

[11] S. Gökceli, T. Levanen, J. Yli-Kaakinen, T. Riihonen, M. Renfors, and M. Valkama, "PAPR reduction with mixed-numerology OFDM," *IEEE Wireless Commun. Lett.*, vol. 9, no. 1, pp. 21–25, Jan. 2019.

[12] X. Liu, X. Zhang, J. Xiong, F. Gu, and J. Wei, "An enhanced iterative clipping and filtering method using time-domain kernel matrix for PAPR reduction in OFDM systems," *IEEE Access*, vol. 7, pp. 59466–59476, 2019.

[13] Y. Wang, M. Wang, and Z. Xie, "A PAPR reduction method with EVM constraints for OFDM systems," *IEEE Access*, vol. 7, pp. 171830–171839, 2019.

[14] B. Tang, K. Qin, X. Zhang, and C. Chen, "A clipping-noise compression method to reduce PAPR of OFDM signals," *IEEE Commun. Lett.*, vol. 23, no. 8, pp. 1389–1392, Aug. 2019.

[15] K. Anoh, C. Tanriover, B. Adebisi, and M. Hammoudeh, "A new approach to iterative clipping and filtering PAPR reduction scheme for OFDM systems," *IEEE Access*, vol. 6, pp. 17533–17544, 2018.

[16] S. Lin, Y. Chen, and S. Tseng, "Iterative smoothing filtering schemes by using clipping noise-assisted signals for PAPR reduction in OFDM-based carrier aggregation systems," *IET Commun.*, vol. 13, no. 6, pp. 802–808, Apr. 2019.

[17] S. Traverso, "A new family of filters for PAPR reduction of carrier aggregated signals," in *Proc. IEEE Wireless Commun. Netw. Conf.*, Doha, Qatar, Apr. 2016, pp. 1–6.
[18] X. Liu, L. Zhang, J. Xiong, X. Zhang, L. Zhou, and J. Wei, "Peak-to-average power ratio analysis for OFDM-based mixed-numerology transmissions," *IEEE Trans. Veh. Technol.*, vol. 69, no. 2, pp. 1802–1812, Feb. 2020.
[19] X. Liu *et al.*, "PAPR reduction using iterative clipping/filtering and ADMM approaches for OFDM-based mixed-numerology systems," *IEEE Trans. Wireless Commun.*, vol. 19, no. 4, pp. 2586–2600, Apr. 2020.
[20] D. R. Morgan, Z. Ma, J. Kim, M. G. Zierdt, and J. Pastalan, "A generalized memory polynomial model for digital predistortion of RF power amplifiers," *IEEE Trans. Signal Process.*, vol. 54, no. 10, pp. 3852–3860, Oct. 2006.
[21] A. Brihuega *et al.*, "Piecewise digital predistortion for mmWave active antenna arrays: Algorithms and measurements," *IEEE Trans. Microw. Theory Techn.*, vol. 68, no. 9, pp. 4000–4017, Sep. 2020.
[22] H. Ochiai and H. Imai, "Performance analysis of deliberately clipped OFDM signals," *IEEE Trans. Commun.*, vol. 50, no. 1, pp. 89–101, Jan. 2002.
[23] S. Gökceli *et al.*, "SDR prototype for clipped and fast-convolution filtered OFDM for 5G new radio uplink," *IEEE Access*, vol. 8, pp. 89946–89963, 2020.
[24] *New Radio (NR); Base Station (BS) Radio Transmission and Reception, Technical Specification Group Radio Access Network, Rel. 16*, 3GPP Standard TS 38.104, Jul. 2019.
[25] A. B. Kihero, M. S. J. Solaija, and H. Arslan, "Inter-numerology interference for beyond 5G," *IEEE Access*, vol. 7, pp. 146512–146523, 2019.
[26] H. Sorensen, M. Heideman, and C. Burrus, "On computing the split-radix FFT," *IEEE Trans. Acoust., Speech, Signal Process.*, vol. 34, no. 1, pp. 152–156, Feb. 1986.
[27] *Specifications VST PXIe-5840*, Nat. Instrum., Austin, TX, USA, 2018. [Online]. Available: http://www.ni.com/pdf/manuals/376626c.pdf
[28] *ZFL-2500VH+ Medium Power Amplifier*, Mini Circuits, Brooklyn, NY, USA, 2020. [Online]. Available: http://www.minicircuits.com/pdfs/ZFL-2500VH+.pdf
[29] *NR; Physical Channels and Modulation, Technical Specification Group Radio Access Network, Rel. 16 V16.0.0*, 3GPP Standard TS 38.211, Jan. 2020.
[30] *NR; Base Station (BS) Conformance Testing Part 1: Conducted Conformance Testing, Technical Specification Group Radio Access Network, Rel. 16 V16.1.0*, 3GPP Standard TS 38.141-1, Jan. 2020.
[31] A. Brihuega, L. Anttila, M. Abdelaziz, T. Eriksson, F. Tufvesson, and M. Valkama, "Digital predistortion for multiuser hybrid MIMO at mmWaves," *IEEE Trans. Signal Process.*, vol. 68, pp. 3603–3618, May 2020.

SELAHATTIN GÖKCELI (Member, IEEE) received the B.Sc. and M.Sc. degrees in electronics and communication engineering from Istanbul Technical University, Istanbul, Turkey, in 2015 and 2017, respectively. He is currently pursuing the D.Sc. degree with the Department of Electrical Engineering, Tampere University, Tampere, Finland.

His research interests include software-defined radio implementations, waveform design for 5G NR, PAPR reduction, and machine learning/artificial intelligence applications for physical layer of 5G NR.

TONI LEVANEN (Member, IEEE) received the M.Sc. and D.Sc. degrees from the Tampere University of Technology, Finland, in 2007 and 2014, respectively.

He is currently with the Department of Electrical Engineering, Tampere University. In addition to his contributions in academic research, he has worked in industry on wide variety of development and research projects. His current research interests include physical-layer design for 5G NR, interference modeling in 5G cells, and high-mobility support in millimeter-wave communications.

TANELI RIIHONEN (Member, IEEE) received the D.Sc. degree (Hons.) in electrical engineering from Aalto University, Helsinki, Finland, in August 2014.

From September 2005 to December 2017, he held various research positions with the School of Electrical Engineering, Aalto University. From November 2014 to December 2015, he was a Visiting Associate Research Scientist and an Adjunct Assistant Professor with Columbia University, New York, NY, USA. He is currently an Assistant Professor (tenure track) with the Faculty of Information Technology and Communication Sciences, Tampere University, Tampere, Finland. His current research interests include physical-layer OFDM(A), multiantennas, and relaying and full-duplex wireless techniques, especially the evolution of beyond 5G systems.

Dr. Riihonen was a recipient of the Finnish Technical Sector's Award for the best doctoral dissertation of the year in Finland within all engineering sciences and the EURASIP Best Ph.D. Thesis Award 2017. He has been nominated 11 times as an Exemplary/Top Reviewer of various IEEE journals. He served as an Editor for IEEE COMMUNICATIONS LETTERS from October 2014 to January 2019. He has been serving as an Editor for IEEE WIRELESS COMMUNICATIONS LETTERS since May 2017.

JUHA YLI-KAAKINEN received the Diploma Engineering degree in electrical engineering and the Doctor of Technology degree (Hons.) from the Tampere University of Technology (TUT), Tampere, Finland, in 1998 and 2002, respectively.

Since 1995, he has held various research positions with TUT. His research interests are in digital signal processing, especially in digital filter and filter-bank optimization for communication systems and very large-scale integration implementations.

ALBERTO BRIHUEGA (Graduate Student Member, IEEE) received the B.Sc. and M.Sc. degrees in telecommunications engineering from Universidad Politécnica de Madrid, Spain, in 2015 and 2017, respectively. He is currently pursuing the Ph.D. degree with Tampere University, Finland,

He is a Researcher with the Department of Electrical Engineering, Tampere University. His research interests include statistical and adaptive digital signal processing for compensation of hardware impairments in large-array antenna transceivers.

MATIAS TURUNEN (Student Member, IEEE) is currently pursuing the M.Sc. degree in electrical engineering with Tampere University (TAU), Tampere, Finland.

He is currently a Research Assistant with the Department of Electrical Engineering, TAU. He is currently with the Faculty of Information Technology and Communication Sciences, TAU, as a University Instructor. His current research interests include in-band full-duplex radios with an emphasis on analog RF cancellation, OFDM radar, 5G new radio systems, software-defined radios, 5G-related RF measurements, and digital signal processing for radio transceiver linearization.

MARKKU RENFORS (Life Fellow, IEEE) received the D.Tech. degree from the Tampere University of Technology (TUT), Tampere, Finland, in 1982.

Since 1992, he has been a Professor with the Department of Electronics and Communications Engineering, TUT, where he was the Head from 1992 to 2010. His research interests include filter-bank-based multicarrier systems and signal processing algorithms for flexible communications receivers and transmitters.

Prof. Renfors was a co-recipient of the Guillemin Cauer Award (together with T. Saramäki) from the IEEE Circuits and Systems Society in 1987.

MIKKO VALKAMA (Senior Member, IEEE) received the M.Sc. and D.Sc. degrees (Hons.) in electrical engineering from the Tampere University of Technology (TUT), Tampere, Finland, in 2000 and 2001, respectively. His Ph.D. dissertation was focused on advanced I/Q signal processing for wideband receivers: models and algorithms.

In 2003, he was a Visiting Postdoctoral Research Fellow with the Communications Systems and Signal Processing Institute, San Diego State University, San Diego, CA, USA. He is currently a Full Professor and the Department Head of Electrical Engineering with Tampere University, Tampere. His current research interests include radio communications, radio localization, and radio-based sensing, with particular emphasis on 5G and beyond mobile radio networks.

Dr. Valkama was a recipient of the Best Ph.D. Thesis Award of the Finnish Academy of Science and Letters for his Ph.D. dissertation.